

**CFD ANALYSIS AND MOLECULAR KINETICS IN A SUPERCRITICAL CO<sub>2</sub>  
CIRCUIT BREAKER**

A Dissertation  
Presented to  
The Academic Faculty

By

Joy Metzler

In Partial Fulfillment  
of the Requirements for the Degree  
Master of Science in the  
College of Engineering  
Daniel Guggenheim School of Aerospace Engineering

Georgia Institute of Technology

December 2024

© Joy Metzler 2024

**CFD ANALYSIS AND MOLECULAR KINETICS IN A SUPERCRITICAL CO<sub>2</sub>  
CIRCUIT BREAKER**

Thesis committee:

Dr. Juergen Rauleder  
Aerospace Engineering  
*Georgia Institute of Technology*

Dr. Joseph Oefelein  
Aerospace Engineering  
*Georgia Institute of Technology*

Dr. Lukas Graber  
Electrical and Computer Engineering  
*Georgia Institute of Technology*

Date approved: December 4, 2024

I do not know what I may appear to the world, but to myself I seem to have been only like a boy playing on the sea-shore, and diverting myself in now and then finding a smoother pebble or a prettier shell than ordinary, whilst the great ocean of truth lay all undiscovered before me.

*Isaac Newton*

To my husband and my family

To God for revealing some small part of His creation to me

## ACKNOWLEDGMENTS

The author would like to thank the members of her thesis committee for their help in preparation of this work – Dr. Rauleder, Dr. Graber, and Dr. Oefelein.

Special thanks are due to the friends and colleagues who made this work possible, specifically to Zoe Wong for allowing the author to tag along on her project as well as Kenjiro Lay and Braulio Vera-Garcia for helping with the author’s dry runs.

The author gratefully acknowledges the support for this work offered by ARPA-e and EMA3D®, in particular Dr. Kevin-Druis Merenda, Mr. Jacob Johnson, and Ms. Emilie LaVoie-Ingram.

This research was supported in part by the Department of Energy, ARPA-E under the project ”TESLA: Tough and Ecological Supercritical Line Breaker for AC.” This research was also supported in part through research cyberinfrastructure resources and services provided by the Partnership for an Advanced Computing Environment (PACE) at the Georgia Institute of Technology, Atlanta, Georgia, USA.

Any views and conclusions contained herein are those of the author, and do not necessarily represent the official positions, express or implied, of the funders. The views expressed in this thesis are those of the author and do not reflect the official policy or position of the US Air Force, Department of Defense or the US Government.

## TABLE OF CONTENTS

<b>Acknowledgments</b> . . . . .	v
<b>List of Tables</b> . . . . .	viii
<b>List of Figures</b> . . . . .	ix
<b>Summary</b> . . . . .	xiii
<b>Chapter 1: Introduction and Background</b> . . . . .	1
1.1 Motivation . . . . .	1
1.1.1 TESLA . . . . .	1
1.1.2 scCO <sub>2</sub> as an Arc Quenching Medium . . . . .	2
1.2 Objectives . . . . .	3
<b>Chapter 2: Methodology</b> . . . . .	4
2.1 EMA3D Charge Plus® . . . . .	4
2.1.1 Solver Settings . . . . .	4
2.1.2 Geometry Set-up . . . . .	6
2.1.3 Numerical Set-up . . . . .	12
<b>Chapter 3: Results - Parallel Plates</b> . . . . .	14
3.1 Investigation of Factors Affecting Run Time . . . . .	14

3.2	Investigation of Factors Affecting Voltage Breakdown . . . . .	16
3.3	scCO <sub>2</sub> . . . . .	20
3.3.1	138 Reactions . . . . .	20
3.3.2	176 Reactions . . . . .	22
3.4	Reaction Study . . . . .	24
<b>Chapter 4: Results - Nozzle . . . . .</b>		<b>28</b>
4.1	Mesh Sensitivity Study . . . . .	28
4.2	scCO <sub>2</sub> . . . . .	31
4.2.1	Investigation of Contact Distances . . . . .	31
4.3	Reaction Studies . . . . .	32
<b>Chapter 5: Discussion . . . . .</b>		<b>39</b>
5.1	Future Work . . . . .	39
5.1.1	Model Improvements . . . . .	39
5.1.2	Topics of Interest . . . . .	40
5.2	Further Application to Relevant Fields . . . . .	41
<b>Chapter 6: Conclusion . . . . .</b>		<b>43</b>
<b>Appendices . . . . .</b>		<b>44</b>
	Appendix A: Full List of Reactions Ordered by Type . . . . .	45
<b>References . . . . .</b>		<b>52</b>

## LIST OF TABLES

2.1	Fluid Properties for STP CO <sub>2</sub> and scCO <sub>2</sub> . . . . .	5
3.1	Critical Electron Density and Breakdown Voltage of Conclusive Tests . . . . .	18
A.1	Cross-sectional Collision Reactions . . . . .	45
A.1	Continued . . . . .	46
A.1	Continued . . . . .	47
A.1	Continued . . . . .	48
A.1	Continued . . . . .	49
A.1	Continued . . . . .	50
A.1	Continued . . . . .	51
A.1	Continued . . . . .	52

## LIST OF FIGURES

2.1	Simulation Mesh - Nozzle . . . . .	7
2.2	3D Nozzle with Nozzle Removed . . . . .	7
2.3	Slice of Nozzle Geometry . . . . .	8
2.4	Simulation Mesh - Parallel Plates . . . . .	11
2.5	Slice of Parallel Plates Geometry . . . . .	12
3.1	Mesh Sensitivity Study . . . . .	14
3.2	Test With Varying Time Steps . . . . .	15
3.3	Test With Varying Initial Electron Densities . . . . .	17
3.4	Trends of Breakdown Voltage and Critical Electron Density . . . . .	17
3.5	Test With Varying Time Steps . . . . .	19
3.6	Test With Varying Time Steps . . . . .	21
3.7	Energy Loss Due to Different Reactions[17] . . . . .	22
3.8	Test With Varying Time Steps . . . . .	23
3.9	Effects of Removing Categories of Reactions - Potential	
	Each curve shows the values predicted if all rates are considered EXCEPT for the one reaction by which it is named . . . . .	25

3.10	Effects of Removing Categories of Reactions - Electron Density	
	Each curve shows the values predicted if all rates are considered EXCEPT for the one reaction by which it is named . . . . .	26
3.11	Effects of Removing Categories of Reactions - Electron Temperature	
	Each curve shows the values predicted if all rates are considered EXCEPT for the one reaction by which it is named . . . . .	27
4.1	Mesh Sensitivity Study . . . . .	28
4.2	Comparison of Breakdown Across Meshes . . . . .	29
4.3	Additional Spikes in Electron Density . . . . .	30
4.4	Investigation of Contact Distances - scCO <sub>2</sub> . . . . .	32
4.5	Investigation of Contact Distances - STP CO <sub>2</sub> (138 Reactions) . . . . .	33
4.6	Investigation of Contact Distances - N <sub>2</sub> . . . . .	34
4.7	Effects of Removing Categories of Reactions - Potential . . . . .	35
4.8	Effects of Removing Categories of Reactions - Electron Density . . . . .	36
4.9	Effects of Removing Categories of Reactions - Electron Temperature . . . . .	37
4.10	Comparison of Breakdown Across Meshes . . . . .	38

## NOMENCLATURE

$\alpha$	Thermal Diffusivity ( $m^2/s$ )
$\gamma$	Second Townsend Coefficient
$\nu$	Kinematic Viscosity
$\rho$	Density ( $kg/m^3$ )
$A$	Ionization Constant ( $cm^{-1}mbar^{-1}$ )
$B$	Ionization Constant ( $B = 350 V/cm^{-1}mbar^{-1}$ )
$C_p$	Specific Heat Capacity ( $J/kg \cdot K$ )
$d$	Gap Distance
$E$	Electric Field ( $V/m$ )
$e^-$	Electrons
$k$	Thermal Conductivity ( $W/m \cdot K$ )
$p$	Pressure
$P_i$	Probability
$t$	Time ( $s$ )
$V_b$	Breakdown Voltage ( $V$ )
CO	Carbon Monoxide

CO<sub>2</sub> Carbon Dioxide

N<sub>2</sub> Nitrogen

O Oxygen

scCO<sub>2</sub> Supercritical Carbon Dioxide

SF<sub>6</sub> Sulfur Hexafluoride

## SUMMARY

In this work, the behavior of supercritical carbon dioxide ( $\text{scCO}_2$ ) at high pressures is investigated in regards to its arc quenching capabilities to suppress reignition in high-voltage circuit breakers.  $\text{scCO}_2$  is a favorable replacement for the current  $\text{SF}_6$  gas, which produces toxic byproducts.  $\text{SF}_6$  contributes heavily to the global warming crisis, and it is paramount to find a more environmentally conscious alternative. One possibility is  $\text{scCO}_2$ , which has a comparable dielectric strength to  $\text{SF}_6$  and shows promise in arc quenching applications; however, the behavior of  $\text{scCO}_2$  is not as well researched as that of  $\text{SF}_6$ , leading to a critical gap in knowledge needed to implement this change. To bridge this gap, a preliminary investigation of  $\text{scCO}_2$  was done using a novel Particle-In-Cell (PIC) solver approach as opposed to a more classic, continuum flow approach. This work presents the initial results from the simulation program Charge Plus[1], developed by Electro-Magnetic Applications Inc. (EMA3D®). Charge Plus is a Particle-In-Cell (PIC) solver that, rather than using fluid properties, instead utilizes reaction probabilities to track macroparticles representing the flow of species in the simulation. While a continuum flow solver is a suitable approach to handle the initial quenching of the arc, the PIC method is particularly suited to answering this work's overarching question of whether restrike (or reignition) will occur due to its leverage of molecular kinetics, as restrike is largely a molecular kinetics problem rather than a thermodynamics problem. Through a series of parametric studies, it was determined that  $\text{scCO}_2$  shows promise preventing arc restrike, but some numerical instabilities and a lack of validation data prevents this work from reaching a conclusive answer to the objective. However, significant progress has been made in building and testing a working model not only for  $\text{scCO}_2$  but also for a nozzle configuration.

# CHAPTER 1

## INTRODUCTION AND BACKGROUND

### 1.1 Motivation

The purpose of this work is to investigate the behavior of an electrical arc when established in supercritical carbon dioxide ( $\text{scCO}_2$ ). Current circuit breakers use  $\text{SF}_6$  due to its high electronegativity and density, making it an effective arc quenching medium for the first strike and in preventing further arc strikes. However, when exposed to moisture,  $\text{SF}_6$  can produce dangerous byproducts like hydrofluoric acid.  $\text{SF}_6$  is also a highly potent greenhouse gas, and its emissions can remain in the atmosphere for up to 3,200 years[2]. Consequently, there is great interest in replacing  $\text{SF}_6$  with a less harmful alternative.

#### 1.1.1 TESLA

$\text{SF}_6$  circuit breakers operate by pulling two fitted contacts apart from each other when the circuit needs to be broken. Due to high currents flowing through the cathode, however, there is enough energy to bridge gaps between the contacts and form an electrical arc that still carry current. To extinguish this arc,  $\text{SF}_6$  is pumped into a chamber surrounding the contacts, where it cools the arc so that the particles deionize and recombine.

TESLA (Tough and Ecological Supercritical Line Breaker for AC) is proposed as an alternative circuit breaker to current  $\text{SF}_6$  designs[3]. It will be built and operated at Georgia Tech and will utilize  $\text{scCO}_2$  rather than  $\text{SF}_6$  as its arc quenching medium.  $\text{scCO}_2$  is chosen for its high dielectric strength. Additionally,  $\text{scCO}_2$  has the advantage of large increases in density for small increases in pressure, making it a better candidate than other supercritical fluids. This high density greatly shortens the fluid's mean free path, giving it potential as a safer and more environmentally friendly candidate to replace  $\text{SF}_6$  in circuit breakers[4].

### 1.1.2 scCO<sub>2</sub> as an Arc Quenching Medium

There have been attempts to understand the behavior of CO<sub>2</sub> as an arc quenching medium, to include experiments[5] and numerical modeling[6], but there are still significant gaps in knowledge when it comes to scCO<sub>2</sub>'s performance. Many current solvers that deal with arc quenching are complex and take a long time to solve. Electrical arcs comprise difficult physics problems, such as plasmas, high temperatures, electric and magnetic fields, and contact ablation, to name a few. Solutions to solve these problems range from implementing large magneto-hydrodynamic (MHD) solvers[7] or through coupling the Navier-Stokes Equations with Maxwell's Equations[8] to 1-D models simplified from conservation equations[9].

These methods that explain the thermodynamics of the system are valuable when answering the question of arc quenching, and there is reasonable confidence that scCO<sub>2</sub> will be able to effectively quench an electrical arc when first formed. This first arc formation is largely a thermodynamics problem, happening on the order of milliseconds and extinguishing through heat transfer away from the arc by injecting scCO<sub>2</sub> into the chamber. This is being studied in separate works by way of the Navier-Stokes equations coupled with the Peng-Robinson equation of state for fluid properties[10]. In this, scCO<sub>2</sub>'s performance is comparable to that of SF<sub>6</sub>, but scCO<sub>2</sub>'s ability to prevent the arc from reigniting is still largely unknown.

Arc restrike or reignition occurs on the order of nanoseconds when excess electrons are emitted from the circuit breaker's heated contacts through field and thermionic emission. Whereas the initial arc quench is dependent on thermodynamic properties of scCO<sub>2</sub>, arc restrike is more dependent on molecular information and reactions, such as the number of electrons emitted and ionization reactions occurring in the system. If a critical electron density is reached, the system can see "electron avalanche," where chain reactions of ionization create enough electrons to reestablish an electrical arc between the contacts. If this happens, there is no way to quench the arc again since the contacts are already separated

with no additional scCO<sub>2</sub> flow, permanently establishing a circuit. Due to SF<sub>6</sub>'s high electronegativity, arc restrike is not as big of a problem as the fluid is able to absorb excess electrons through attachment. scCO<sub>2</sub> does not have as high of an electronegativity and would have to prevent electron avalanche through other means.

For the reasons above, it is imperative to the TESLA project to also understand how scCO<sub>2</sub> handles arc restrike. Most CFD solvers lack the information necessary to predict restrike, as they do not provide information on molecular kinetics. This work proposes the use of a novel method that relies on molecular collision reactions and energy transfer rather than on thermodynamics and fluid properties. This method, called the Particle-in-Cell (PIC) method, monitors a limited number of particles and calculates their interactions with each other through a series of reactions to estimate the densities of the various scCO<sub>2</sub> species over time, to include electrons being produced through ionization or taken out of the system via attachment or other reactions.

## **1.2 Objectives**

The overall purpose of this work is to determine whether restrike of the arc is a possibility based on molecular kinetics. To prevent current from continuing to flow between the breaker contacts, electrons must diffuse quicker through reactions such as recombination and excitation than they are being produced through interactions such as ionization and detachment. As a consequence, understanding the production of electrons in the system is critical to understanding arc restrike. In order to understand the probability of restrike occurring in scCO<sub>2</sub>, the objectives of this work are listed below:

1. After arc quenching, does the electron density continue rising and reestablish connection (restrike) between the two contacts?
2. What are the conditions in the nozzle that contribute to rising electron density?

## CHAPTER 2

### METHODOLOGY

Modeling plasmas present at high temperatures and high pressures is a difficult task that requires capturing many different physical phenomena. Consequently, different methods of solving can be used to tackle different angles of the same problem. Charge Plus is a numerical solver that uses a Monte Carlo Collision method with a PIC method to calculate plasma dynamics. This program is actively under development, and its target application is circuit breakers and arc quenching. This makes it a good candidate for the problem presented in this work.

#### 2.1 EMA3D Charge Plus®

##### 2.1.1 Solver Settings

In a plasma, there are interactions between particles that are important to include in calculations, and this is achieved using the Monte Carlo Collision (MCC) method. The MCC method is outlined by Vahedi et al.[11], in which the full process is explained in detail.

A collision can be described by its probability of happening and by type of collision. Probability is based on a particle's kinetic energy, which affects its collision cross section, and is defined as  $P_i$ . In the solver, if a uniformly distributed random number on the interval  $[0, 1]$  is less than  $P_i$ , then a collision has occurred. Another random number is chosen to determine the type of collision that occurs (e.g. elastic scattering, excitation, ionization). Finally, once the information of this collision is determined, other information such as scattering angle of the particle can be determined, and the simulation is updated based on the reaction that occurred.

The species that are part of this simulation are  $e^-$ , CO, C, O, O<sub>2</sub>, O<sub>3</sub>, CO<sub>2</sub><sup>+</sup>, CO<sup>+</sup>, C<sup>+</sup>,

$O^+$ ,  $O_2^+$ ,  $O^-$ ,  $O_2^-$ , and  $O_3^+$ . These neutral and ion species can be defined either as fluid species or PIC species, but in this work, the only species defined as a fluid is neutral  $CO_2$ . While fluid properties can be gained from the solver, the time scales are too short to see meaningful change in the fluid properties of  $CO_2$ .

To define a fluid, the solver needs values for its initial density, kinematic viscosity ( $\mu$ ), and thermal diffusivity. Thermal diffusivity ( $\alpha$ ) is defined as a function of specific heat capacity ( $C_p$ ), density ( $\rho$ ), and thermal conductivity ( $k$ ).

$$\alpha = \frac{k}{C_p \rho} \quad (2.1)$$

The advantage of the Charge Plus method is that the solver only needs transport properties at a given pressure along an isothermal line, in this case around 300 K. Properties for  $CO_2$  are provided by the NIST WebBook[12] and are tabulated in Table 2.1.

Table 2.1: Fluid Properties for STP  $CO_2$  and sc $CO_2$

Pressure	Temperature (K)	$\rho$ (kg/m <sup>3</sup> )	$\nu$ (m <sup>2</sup> /s)	$\alpha$ (m <sup>2</sup> /s)
1 atm (STP)	300 K	1.78	8.47E-6	1.11E-5
10 MPa (sc)	305 K	751.67	8.46E-8	7.13E-7

Collisions dictate the state of the simulation over time and happen according to the probabilities calculated by the MCC. The original set of reactions (138 total) was provided by EMA3D®, compiled from work done by Allati[13], Berthelot[14], and Koelman[15]. Additional reactions were found directly from immediate availability on LXCat, along with the actual cross-sectional data. Appendix A includes a full description of the reactions included, categorized by type.

Cross-sectional data is used to determine the likelihood of a collision happening. These are given over a range of energies, and in the case of excitement cross-sections, multiple energy levels are provided to the solver. Reactions with larger cross-sectional areas are more likely to occur.

Additionally, some reactions can be modeled by other means other than cross-sections. Some supported methods are the Townsend model, the Arrhenius model, a rate coefficient, or a rate constant. These are also listed in Appendix A by type of reaction along with their associated value included in the solver.

There are three main assumptions that the solver makes.

1. The gas only interacts with itself through elastic collisions.
2. The main interaction is between the plasma and neutral particles.
3. The fluid is an ideal gas and follows ideal gas relations.

It also assumes a Maxwellian distribution for both PIC and fluid species in its collision model, though the user can choose different distributions.

### 2.1.2 Geometry Set-up

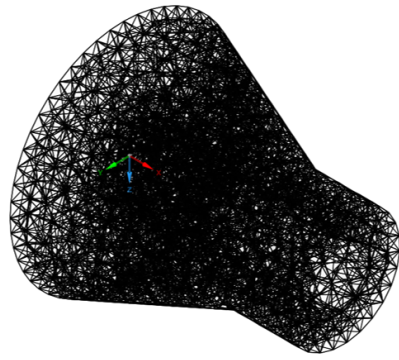
Charge Plus utilizes a combination of unique and familiar boundary conditions. The model is first designed using Ansys Discovery and meshed using Discovery's native meshing software. The cells are unstructured tetrahedrals, and the cell size can be set to a preferred value.

#### *Nozzle*

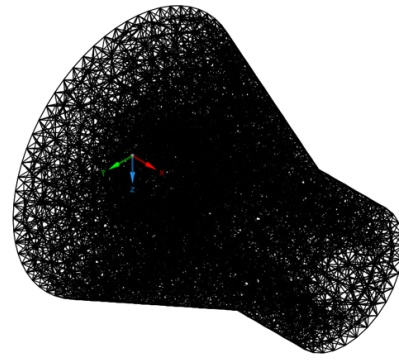
The full mesh model is shown in Figure 2.1. Smaller mesh sizes result in cells that are smaller but still identically shaped.

The physical model consists of a nozzle model combined with an anode and a wholly separate cathode body. The model is fully 3D, as shown in Figure 2.2.

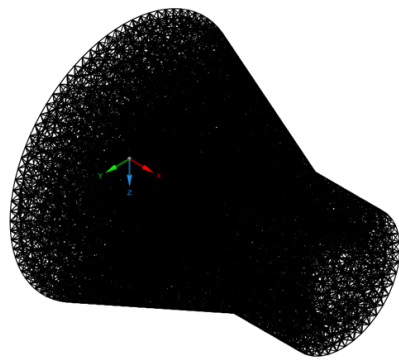
The cathode body fits into a gap in the nozzle, but the cathode is removed in Figure 2.2 to show the separate bodies. A slice of the model with numbered points of interest is shown in Figure 2.3 with the cathode remaining in the body.



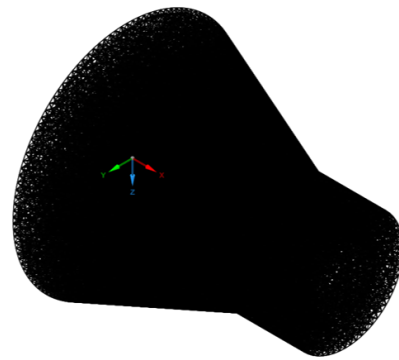
(a) 0.005 m



(b) 0.004 m

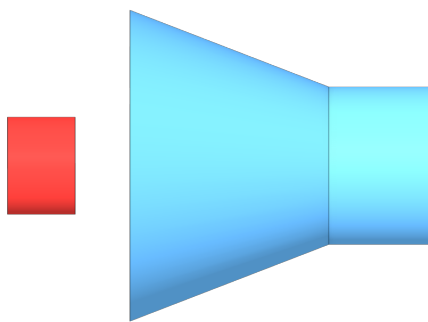


(c) 0.003 m

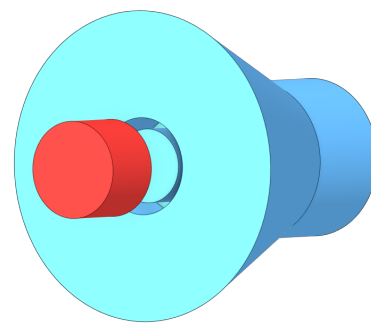


(d) 0.002 m

Figure 2.1: Simulation Mesh - Nozzle



(a)



(b)

Figure 2.2: 3D Nozzle with Nozzle Removed

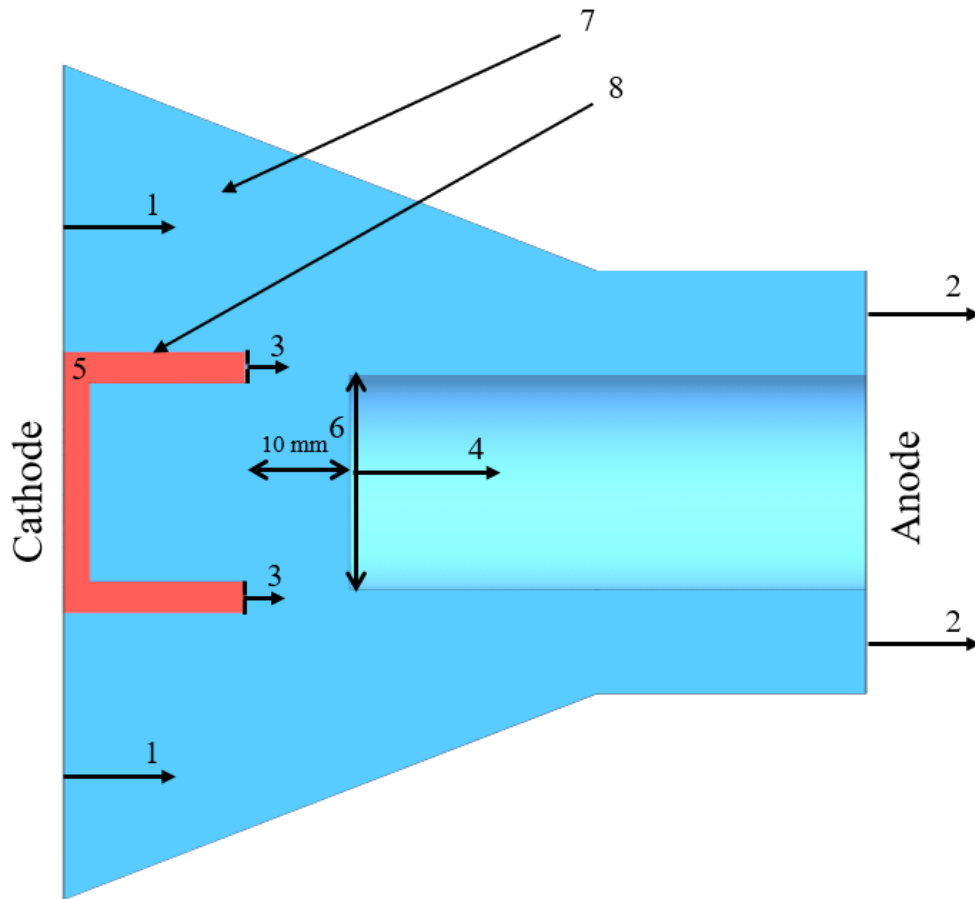


Figure 2.3: Slice of Nozzle Geometry

The model includes two sets of inlets and outlets, and these are defined as boundary conditions. One set is for the fluid (1 and 2), and the other is for the electrons (3 and 4). The fluid inlet defines where fluid species flow in, to include neutrals and ions, and an initial velocity can also be defined here. The fluid outlet allows those fluid species to exit the computational domain, also at some defined exit velocity. Similarly, an electron inlet and outlet allows electrons to move in from the anode and out through the cathode. Positive ions have the same inlets and outlets as the neutral fluids, and negative ions flow in the same direction as the electrons. These inlets and outlets were not properly functioning as of publication of this work, so while the results presented do not include the full effects of inlets and outlets, they have a nontrivial effect and will eventually need to be included. The one inlet that is still included is an electron inlet placed at 4, and this is meant to help maintain the number of electrons in the simulation. In this work, this value is always set to the initial electron density, which represents electrons emitted through field emission, thermionic emission, or from other sources.

In an industrial circuit breaker, a contact has a 50% chance of being the cathode, depending on when the circuit is broken. As this is a static simulation, these conditions had to be assumed. A current source is applied on the cathode body (5), which is assumed to be the tulip shaped contact, and allows a current to be prescribed at a given surface. In this work, the current source's signal is a simple linear ramp-up, where the current reaches a peak amplitude in a certain amount of time. The current amplitude (given in Amps) is converted to  $A/m^3$  and distributed across the volume of each mesh element in the cathode. It is most similar to a voltage source and could be related through a known resistance of the contacts. The current source is different from the actual current of the arc, and the current source will continuously be applied to the cathode unless specified otherwise as an input. The purpose of this current source is to create a potential difference across the gap.

The anode is assumed to be the cylindrical space starting from 6 and extending to the end of the simulation space, and it is set to a constant value of 0 V. The distance between the

cathode and the anode is 10 mm for validation purposes, but this distance can be lengthened or shortened to account for the opening of the two contacts.

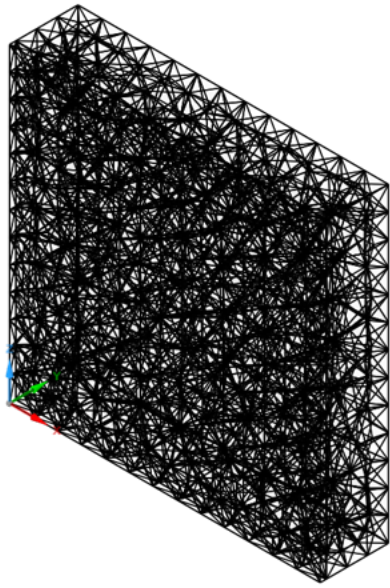
Body materials can be solid materials or fluid space. On the cathode, the body material can be set to a metal (8), though this is only to let the solver know that no species are allowed to exist within that space. The material most used in circuit breakers is a copper-tungsten metal matrix composite, but this is more important when considering thermionic emission effects. In this work, the solver does not take specific material properties into account, and it functions as just another boundary condition. Conversely, the nozzle body (7) is set to allow electrons and fluid or PIC species to exist and interact in the open space. Additionally, the surface of the nozzle is assumed to be insulating, so the electric field vector ( $\vec{E}$ ) is set to 0 everywhere on the outer surface of the model.

### *Parallel Plates*

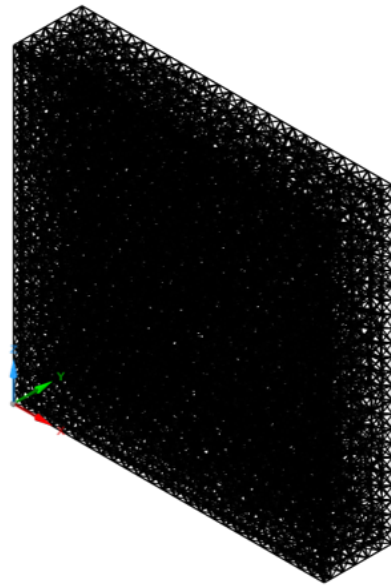
The parallel plates case is set up very similarly to the nozzle, but rather than a solid enclosure, the boundary conditions are set to recreate an infinite set of plates, similar to the case Paschen's Law describes. The mesh for the parallel plates case is shown in Figure 2.4.

The parallel plates are set up very similarly to the nozzle case, and this is briefly reviewed in Figure 2.5.

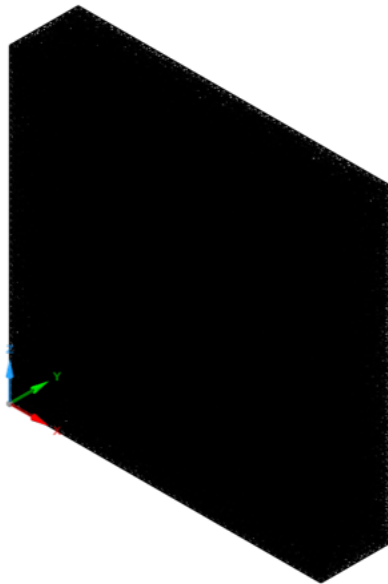
Just like the nozzle, the cathode is a separate body from the anode with a 10 mm gap in between. Whereas the nozzle had distinct geometries for its contacts, the parallel plates simply have one face as the anode (2, 3) and the other face as the cathode (1, 4). The current source is applied to the cathode body (5) to create a potential difference. The cathode body is assumed to be aluminum (8), and the space in between is set so species can exist within the gap (7).



(a) 0.004 m



(b) 0.002 m



(c) 0.001 m

Figure 2.4: Simulation Mesh - Parallel Plates

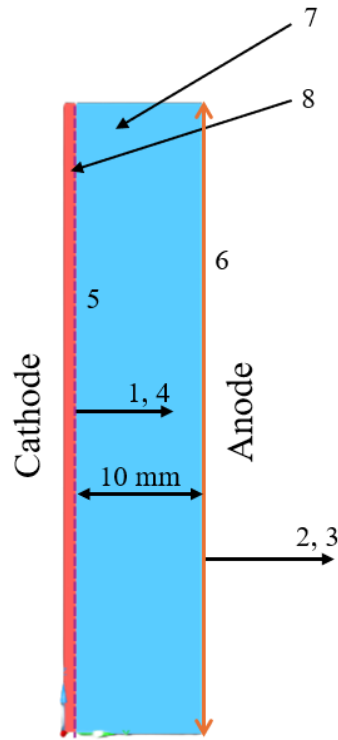


Figure 2.5: Slice of Parallel Plates Geometry

### 2.1.3 Numerical Set-up

For the PIC solver, other parameters can be defined that control the PIC method. The statistical measure is a measure of how many "macro" particles the solver uses to represent the flow of electrons. This can be on the order of millions to billions, depending on desired accuracy, where increasing the statistical measure will slow the simulation but provide a more accurate result. The statistical measure used in this work is  $5e5$ .

The behavior of electrons is also defined for the PIC method. Electrons can either be set to "replace" or "reflect". When set to "replace", an electron will move out of the simulation space and be replaced by more electrons at some rate determined by a number between 0% and 100%. Similarly, if set to "reflect", the electrons will not be replaced, but they may still flow out of the simulation space at a rate also determined by a number between 0% and 100%. In this work, electrons and other PIC species are set to reflect at 0%, and this

means that electrons will flow out of the simulation space similarly to the "replace" setting, but they will not be replaced with new electrons.

The PIC solver time step is set to  $1e - 12s$  at the developer's recommendation. Arc formation typically happens on the order of nanoseconds, so simulations are run for anywhere from 50,000 to 100,000 iterations. This number will vary throughout this work due to computational resource availability.

The finite element method (FEM) solver is set to the same time step as the PIC solver, and the PIC method and the FEM solver can be used interchangeably for each species. The fluid solver is currently limited, and it is currently only capable of solving laminar flow. Though the FEM solver can be used with the solver, voltage breakdown happens on orders of magnitude smaller time scales than would be necessary to see fluid properties change via the FEM solver; therefore, this work does not heavily investigate results from the FEM solver.

## CHAPTER 3

### RESULTS - PARALLEL PLATES

To determine the initial conditions for CO<sub>2</sub>, both STP and supercritical, a simplified parallel plates simulation was investigated. The boundary conditions for the parallel plates are setup to simulate a small section of two infinite parallel plates with a uniform electric field between them. This is done so that Paschen's Law can be used as a validation method, as Paschen's law is derived for two infinite plates with a uniform electric field.

#### 3.1 Investigation of Factors Affecting Run Time

The first tests conducted involved a mesh sensitivity test and a time step test. These were conducted in order to understand how these factors affect the simulation results as well as to understand the best way to cut down simulation time and save computational resources.

The mesh sensitivity results for the parallel plates case are shown in Figure 3.1. These tests were conducted with an initial electron density of 1e9 and a current sources of 1 A.

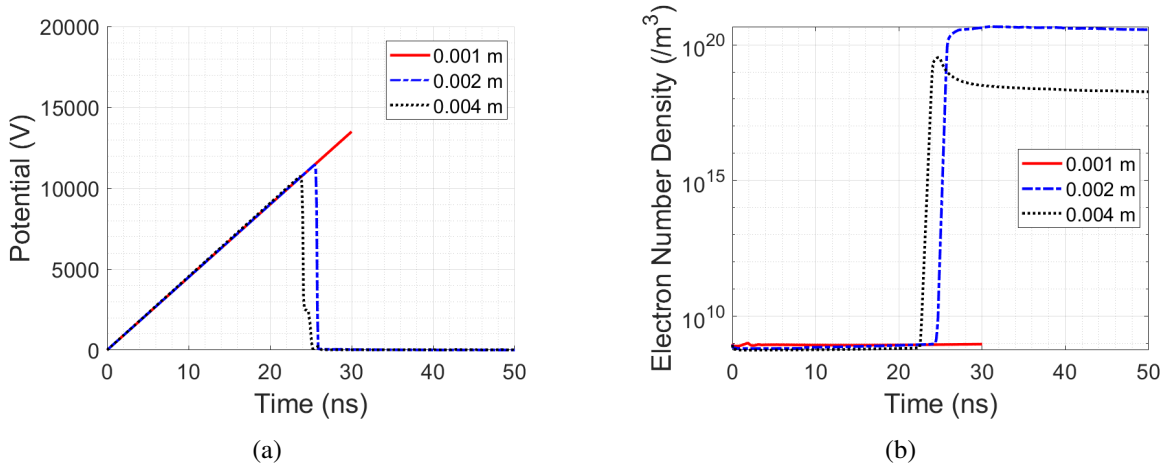


Figure 3.1: Mesh Sensitivity Study

The mesh sizes of 0.002 m and 0.001 m were run for 75,000 iterations while the mesh size of 0.001 m was run for 30,000 iterations. 0.001 m took considerably longer and used

up more computational resources than the more coarse mesh sizes, which is why the case could not be run as long. For the scope of this project, it was determined that the 0.001 m mesh was not feasible to be run. Because the results from the finest mesh are not conclusive, it may be important to run another investigation into mesh size, as using a coarser mesh may be a point of error.

The 0.002 m mesh does show deviance from the 0.004 m case, resulting in a 6.5% increase in breakdown voltage, which corresponds to a 235% increase in the critical electron density. For these reasons, it was determined that the 0.002 m mesh would be the most appropriate to continue running simulations. However, the 0.004 m mesh can provide fast information on trends that are not computationally expensive.

The time step tests are shown in Figure 3.2 and were run at the same conditions as the mesh sensitivity test.

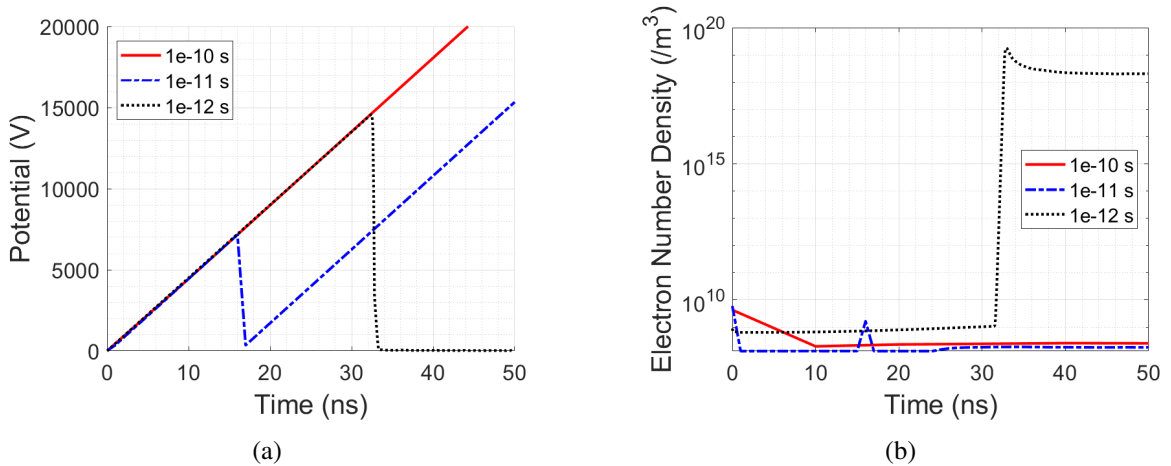


Figure 3.2: Test With Varying Time Steps

Each simulation was run for 50,000 iterations, which affected how many nanoseconds each run lasted. For the sake of comparison, Figure 3.2 is truncated to 50 nanoseconds, which is sufficient to show the differences between the three cases.

Taking a time step of  $1e-12$  s as truth, due to the developer's recommendation, time steps of  $1e-11$  s and  $1e-10$  s were tested to determine whether the simulations could be run at larger time steps. There are a couple indications that a time step at least as small as

1e-12 s is required. The first is found in Figure 3.2a. The breakdown potential for 1e-11 s is more than half the value of 1e-12 s. 1e-10 s does not even experience breakdown. This is further understood by looking at the electron densities in Figure 3.2b. A time step of 1e-12 s produces the expected trend for electron density after breakdown. 1e-10 s drops and gradually increases, which explains why the potential continually increases. It may also be indicative of the solver being unable to capture enough reactions to produce voltage breakdown, which happens on the order of nanoseconds. This is a similar case in 1e-11, though the solver does capture some rise in electrons. It is still not enough to produce and sustain an arc.

Further studies may be necessary to investigate smaller time steps. For the length of this study, it was assumed that  $\Delta t = 1e - 12s$  would be sufficient based on the developer's recommendation and resource limits. However, depending on the stability of the solver, a more in-depth study of the connection between time step and mesh size could be required. Additionally, when adjusting to the high pressures and shorter mean free paths of  $scCO_2$ , there may be physical limitations to how large the time step can be to ensure a significant number of reactions are occurring.

### **3.2 Investigation of Factors Affecting Voltage Breakdown**

While voltage breakdown is one of the most widely readily available methods of validation, it does not give a holistic understanding of the reaction kinetics within the simulation. The breakdown voltage can be dependent on a variety of other factors that are adjustable in the simulation. These include the initial electron density and the cathode current sources. The initial electron density is a value that injects electrons into the simulation until ionization begins occurring. In a circuit breaker, this would be physically represented by field and thermionic effects from extreme heating of the contacts (close to the metal's melting point). As the model matures alongside experiments and other computational models, this value will be closer to the actual number of electrons emitted. Due to a current lack of un-

derstanding, this work seeks to understand how increasing this number of emitted electrons affects the simulation.

The simulation's sensitivity to initial electron density was investigated by increasing the initial electron density by an order of magnitude for seven:  $1.25e7$ ,  $1.5e7$ ,  $1.75e7$ ,  $1e8$ ,  $1e9$ ,  $1e10$ , and  $1e11$ . The results of these tests are shown in Figure 3.3.

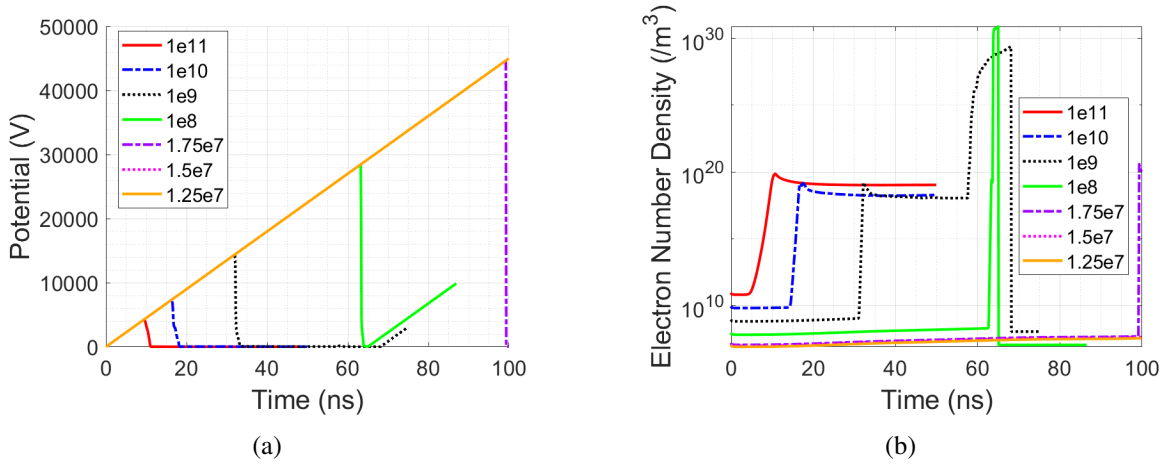


Figure 3.3: Test With Varying Initial Electron Densities

Figure 3.4 shows the trends of parameters of interest as initial electron density is adjusted, and Table 3.1 lists the numerical values of each marker.

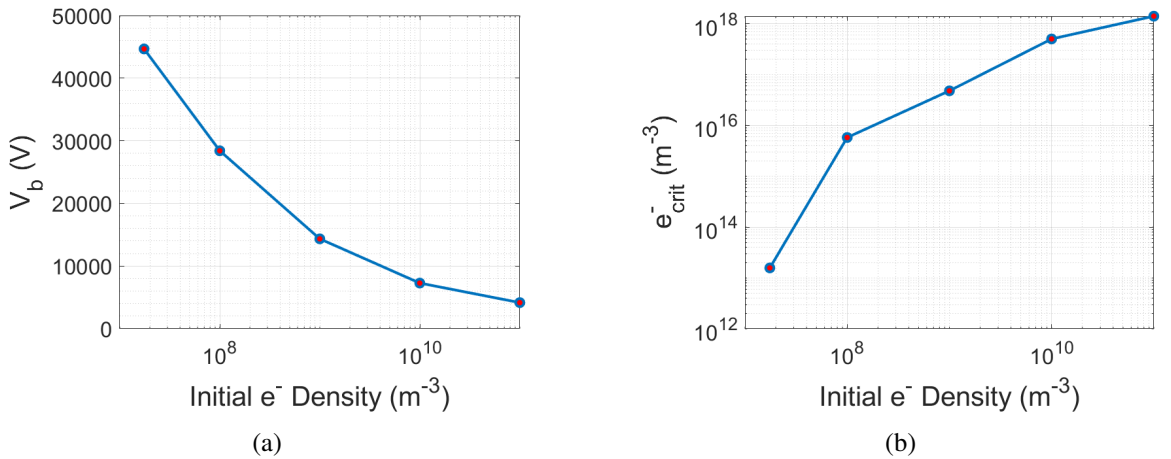


Figure 3.4: Trends of Breakdown Voltage and Critical Electron Density

Table 3.1: Critical Electron Density and Breakdown Voltage of Conclusive Tests

Initial $e^-$ Density ( $\text{m}^{-3}$ )	$e^-_{crit}$ ( $\text{m}^{-3}$ )	$V_b$ (V)
1e11	1.409E18	4,158.1
1e10	5.022E17	7,276.7
1e9	4.795E16	14,341
1e8	5.792E15	28,402
1.75e7	1.576E13	44,665

In order to validate the parallel plate results, the initial electron density is one of the best conditions to adjust. Because there is not sufficient existing literature to conclusively say what the initial electron density should be, this work adjusts the initial electron density so that the breakdown voltage most closely matches the estimation of breakdown voltage by Paschen's Law, given by Equation 3.1, assuming that the original list of reactions is sufficient to describe the energy exchange and ionization of STP  $\text{CO}_2$ .

$$V_B = \frac{Bpd}{\ln(Apd) - \ln[\ln(1 + \frac{1}{\gamma})]} \quad (3.1)$$

Where

$$A = 15 \text{ cm}^{-1}\text{mbar}^{-1}$$

$$B = 350 \text{ V/cm}^{-1}\text{mbar}^{-1}$$

$$\gamma = 0.01 \text{ (for stainless steel electrodes)}$$

for  $\text{CO}_2$  at standard operating conditions[16]. It is important to note that Paschen's Law breaks down at higher pressures, so this validation must be done at STP or lower pressures. With the empirically determined coefficients  $A$  and  $B$ , the estimated breakdown voltage is  $V_b = 43,784 \text{ V}$ . 1.25e7 and 1.5e7 did not reach breakdown in the given amount of time, but based on the general trend of  $V_b$  as the initial electron density decreases, 1.25e7 and 1.5e7

would overshoot the  $V_b$  predicted by Paschen's Law. The initial electron density that most closely reaches that breakdown voltage is  $1.75e7$ , with  $V_b = 44,665V$ .

Interestingly enough,  $1e9$  and  $1e8$  show strange behavior in Figure 3.3b. The reason for  $1e9$ 's behavior is unknown, as it does not seem to have a physical explanation. The behavior of  $1e8$  may be explained by the low amount of electrons in the system. There is a possibility that, when breakdown happens, there are not enough electrons in the system to maintain an arc. It could also be attributed to the solver itself, similar to  $1e9$ . Either way, both cases under predict the correct breakdown voltage.

As the initial electron density increases by an order of magnitude, the time it takes for the system to breakdown decreases. This makes physical sense as a higher concentration of electrons initially in the system will lead to a higher probability of reactions, to include ionization which leads to electron avalanche. The reason the breakdown voltage increases is because the potential continues to build as time goes on, so if breakdown happens at a later time, it will inevitably be greater than a breakdown happening at a sooner time.

Another factor that can increase breakdown voltage is the cathode current source. While this is merely a simulation tool to create a potential difference in the system, a higher current source will cause the potential to increase more sharply and reach higher potentials. The plates' sensitivity to the cathode current source is shown in Figure 3.5.

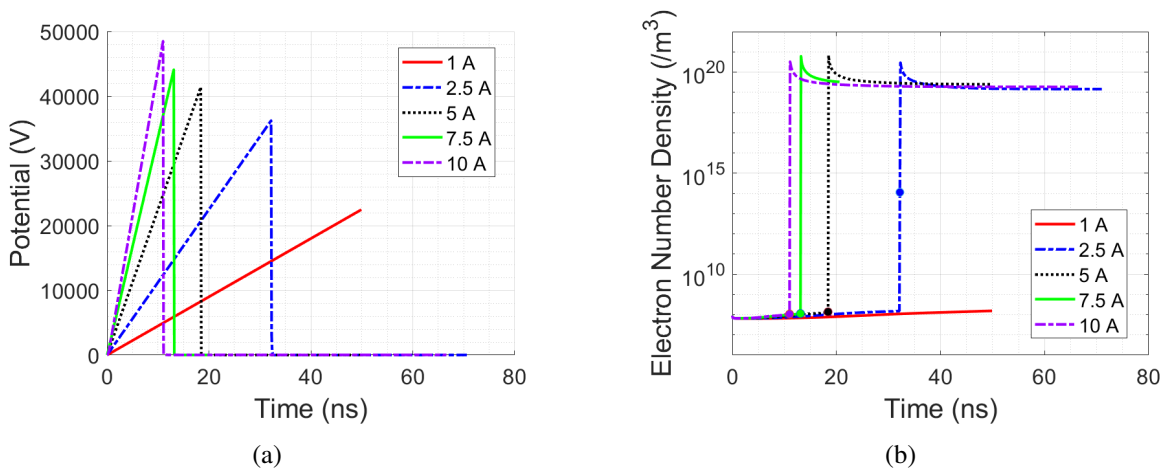


Figure 3.5: Test With Varying Time Steps

While the voltage breakdown changes marginally between runs, the electron density plots show good agreement, with the exception of 2.5 A and 1 A. While 1 A is still inconclusive, the current sources of 5 A, 7.5 A, and 10 A produce a somewhat similar critical electron density, where the greatest percent difference is 22.31%. While this percent difference would normally be considered significant, the critical electron densities are all on the same order of magnitude. Whether or not this drastically affects the behavior of the system is still unknown. The points of electron breakdown, and thus the critical electron density, are shown in Figure 3.5b as colored dots. The points for 5, 7.5, and 10 A are all right at the point before the electron density jumps up, which matches the phenomenon of voltage breakdown. 2.5 A places its voltage breakdown point at a point in the middle of electron avalanche. This is an unexpected result, and it could be a consequence of the small timescales voltage breakdown happens during.

This current source test is important to save computational time, as low current sources take significantly longer to breakdown. Higher current sources will take less computational resources and as shown in Figure 3.5, they also display a similar molecular behavior, although breakdown may happen at a different time. As such, the final current source used for the parallel plates simulations is 10 A.

### **3.3 scCO<sub>2</sub>**

With the initial conditions determined from validating STP CO<sub>2</sub> with Paschen's Law, scCO<sub>2</sub> was investigated in the parallel plates case using this information. All scCO<sub>2</sub> simulations were run with  $\Delta t = 1e - 12s$ , an initial electron density of  $1.75e7$ , and a mesh size of 0.002 m.

#### 3.3.1 138 Reactions

The results from the scCO<sub>2</sub> simulations are mixed, and they may show signs of instability. The first test was done with a set of 138 reactions, shown in Figure 3.6.

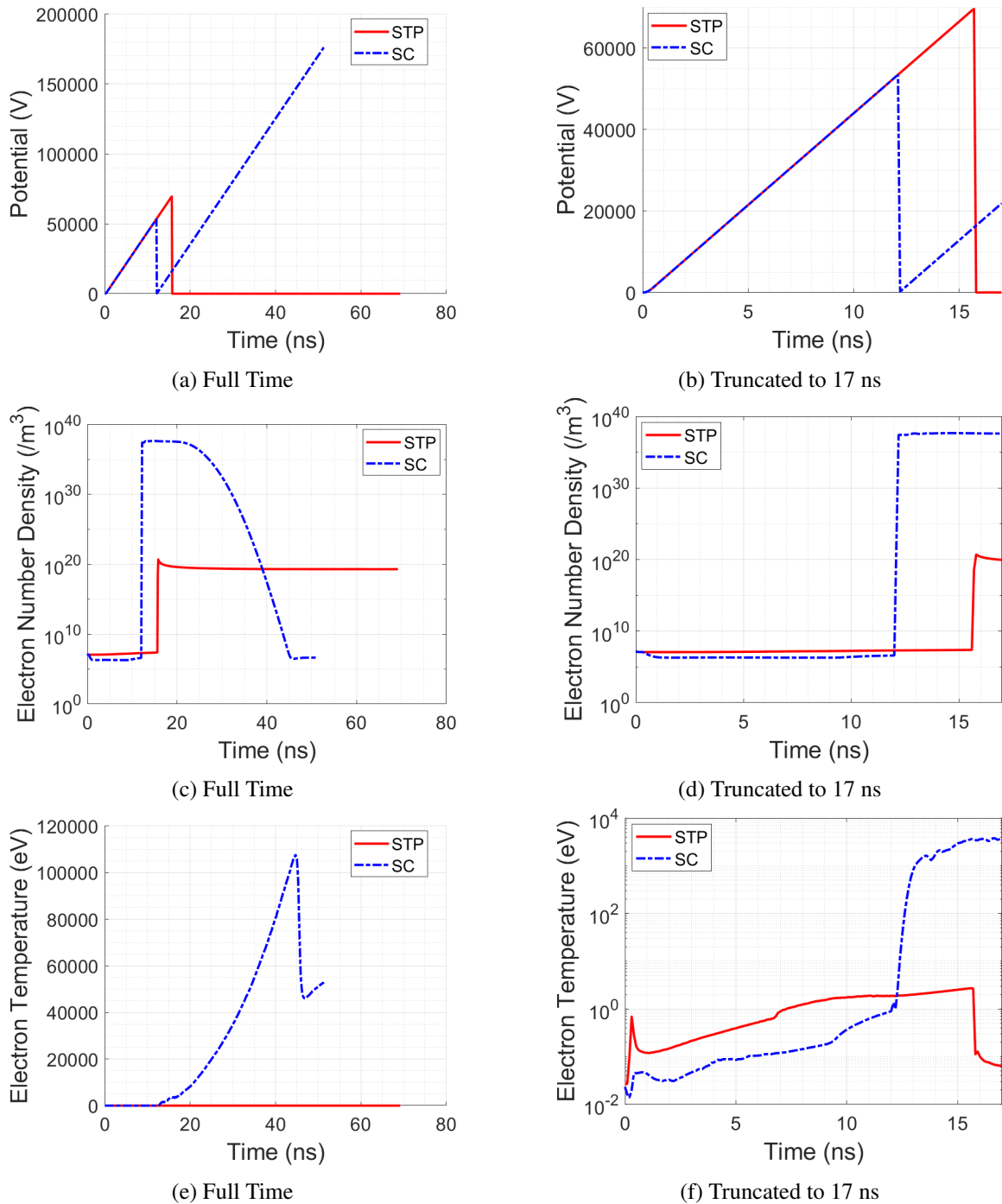


Figure 3.6: Test With Varying Time Steps

The potential of the scCO<sub>2</sub> case vs. the STP CO<sub>2</sub> case seem surprising at first. The expectation is that scCO<sub>2</sub> would breakdown at a higher potential than the STP case. However, earlier tests on the parallel plates show that there are a number of factors that can affect  $V_b$ .

The largest issue presented by these results is the impossible electron temperatures that occur after the initial breakdown. What is promising is, at these initial conditions, scCO<sub>2</sub> breaks down but is unable to maintain a connection between the contacts. On the other hand, the STP case is able to sustain a connection between the contacts. Additionally, the simulation estimates that the scCO<sub>2</sub> case can handle a larger influx of electrons and still not maintain connection. This would match expectations of scCO<sub>2</sub> being a better insulative material, but the increasing electron temperature requires further investigation.

### 3.3.2 176 Reactions

As a result of the results from 138 reactions, the question was raised whether there are enough reactions in the simulation to properly simulation scCO<sub>2</sub>. This is reflected in literature, such as Yong et al.

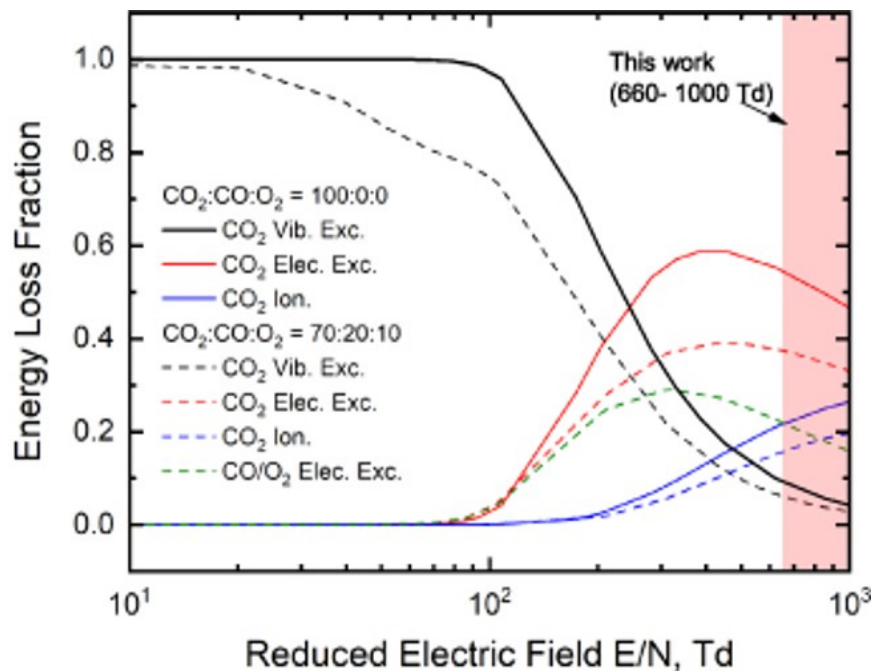


Figure 3.7: Energy Loss Due to Different Reactions[17]

Figure 3.7 demonstrates that, at higher concentrations of neutral articles, electronic excitation becomes non-negligible as a contributor to energy loss. To test whether this, alone, could address some of the issues with the 138 reaction tests, 36 excitation reactions

were added as well as 2 elastic collision reactions (fully outlined in Appendix A). The results are shown in Figure 3.8.

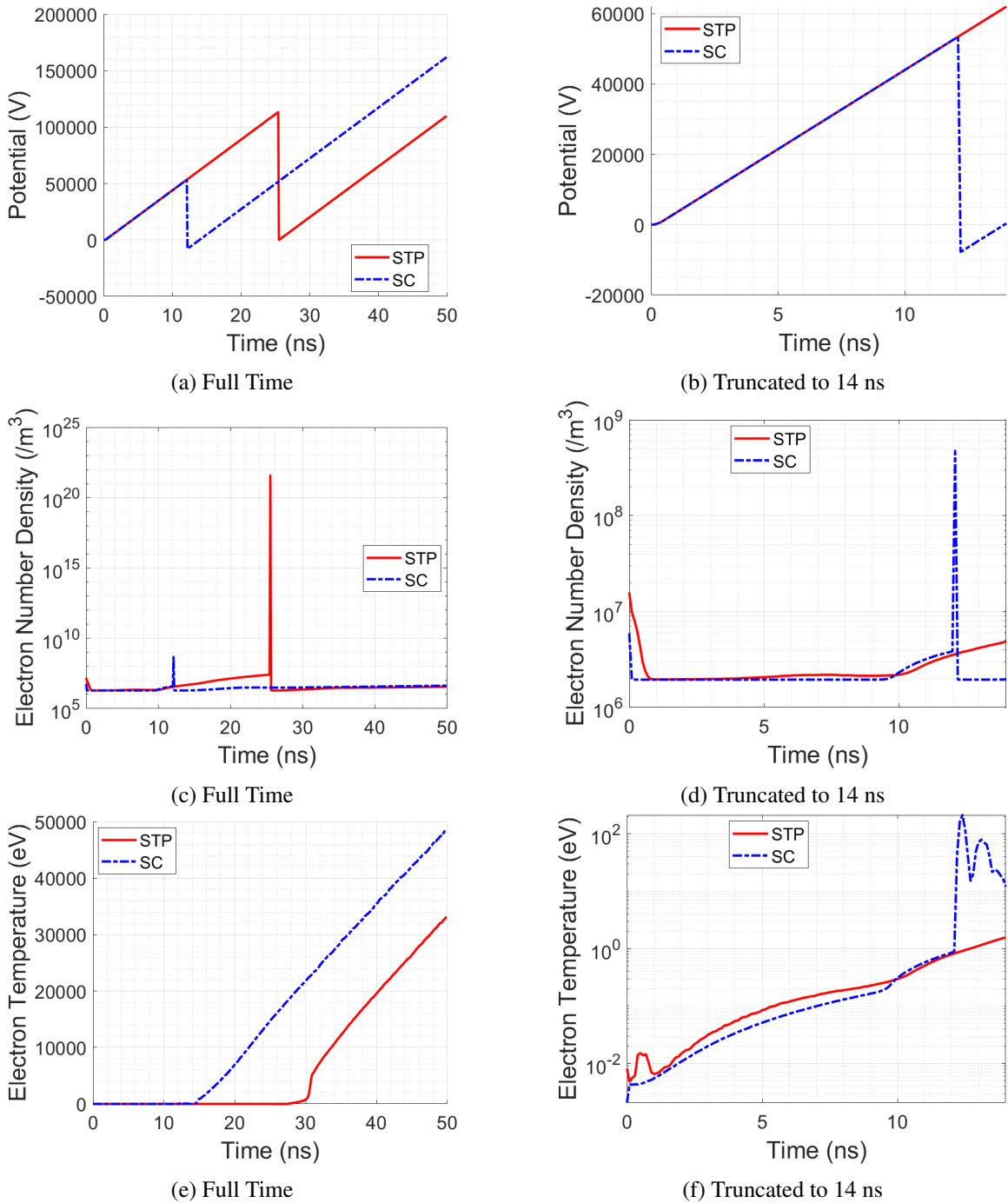


Figure 3.8: Test With Varying Time Steps

Similar to the 138 reactions case, the electron temperature becomes unstable after breakdown, though the  $scCO_2$  case is lower by a couple orders of magnitude. Additionally,

the STP CO<sub>2</sub> case also sees a sharp increase in electron temperature, as well as a non-sustained spike in electron density. This is in contrast to the 138 reactions case, where the STP case broke down and was not able to sustain a high electron density.

Because adding in more reactions did not fully address the discrepancies of these results, there are a couple other possible sources of error that could warrant further study. First, electrons may be building up in the simulation, which may be the source of the high electron temperatures. This could be solved with future releases of the solver, which plans to include electron outlets to allow particles to exit the system through one of the contacts. The other possible source of error could lie in not having enough reactions at high activation energies. This seems to be the more likely error due to the behavior of the simulations from 138 reactions to 176 reactions. As addressed previously, the electron temperature of the scCO<sub>2</sub> case decreased by a couple orders of magnitude with the inclusion of an extra 36 reactions. Additionally, the results stay physical before either simulation breaks down for the first time, so once the system's electrons start gaining energy, they may be unable to release it at higher energy levels due to a lack of excitation reactions.

### **3.4 Reaction Study**

There are 11 types of reactions included in this study: attachment, elastic collisions, detachment, dissociation, excitation, ion-ion collisions, ionization, ion-neutral collisions, neutral-neutral collisions, and recombination. These are categorized in Appendix A. To test the effects of a certain category of reactions on the overall simulation, each category was individually removed from an scCO<sub>2</sub> simulation and then subsequently replaced. As reactions are not independent of each other, this approach was deemed best rather than progressively adding or subtracting reaction categories one-by-one. The results are presented in Figure 3.9, Figure 3.10, and Figure 3.11.

Many of the categories seem to have a negligible effect on the simulation's predictions, but there are a few categories that do have a noticeable effect.

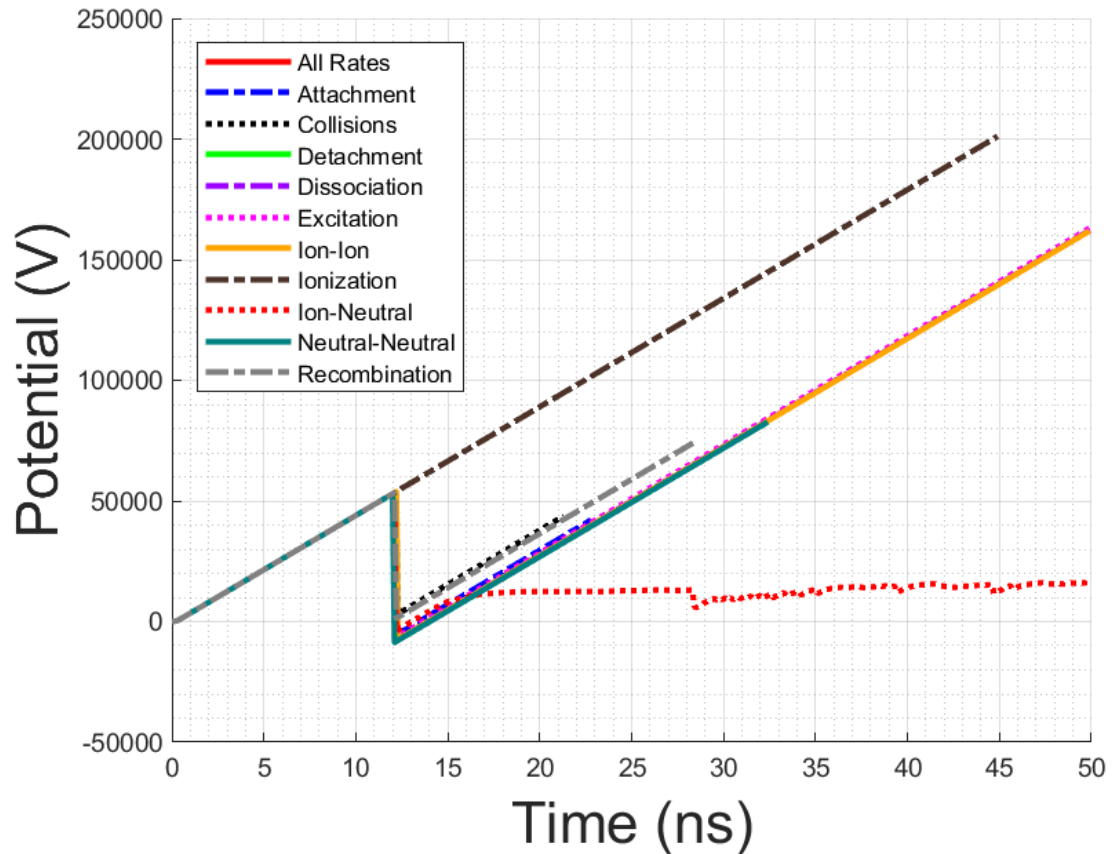


Figure 3.9: Effects of Removing Categories of Reactions - Potential

Each curve shows the values predicted if all rates are considered EXCEPT for the one reaction by which it is named

The first category is the ion-neutral interactions. Removing this category caused the simulation to breakdown and maintain a connection. It also led to the highest electron number density in the simulation and to the lowest electron temperatures. Compared to the effects of removing neutral-neutral and ion-ion reactions, this may suggest that there are not enough neutral-neutral reactions included in the solver, or it may suggest that ion-neutral reactions are important to removing energy from the simulation.

Removing ionization reactions had the expected effect on the simulation, being the only category to prevent breakdown altogether. Without the ability for the solver to create electrons, the electron number density stays largely constant, but the electron temperature sees a spike once the electron temperature surpasses 1 eV. This also seems to be around the

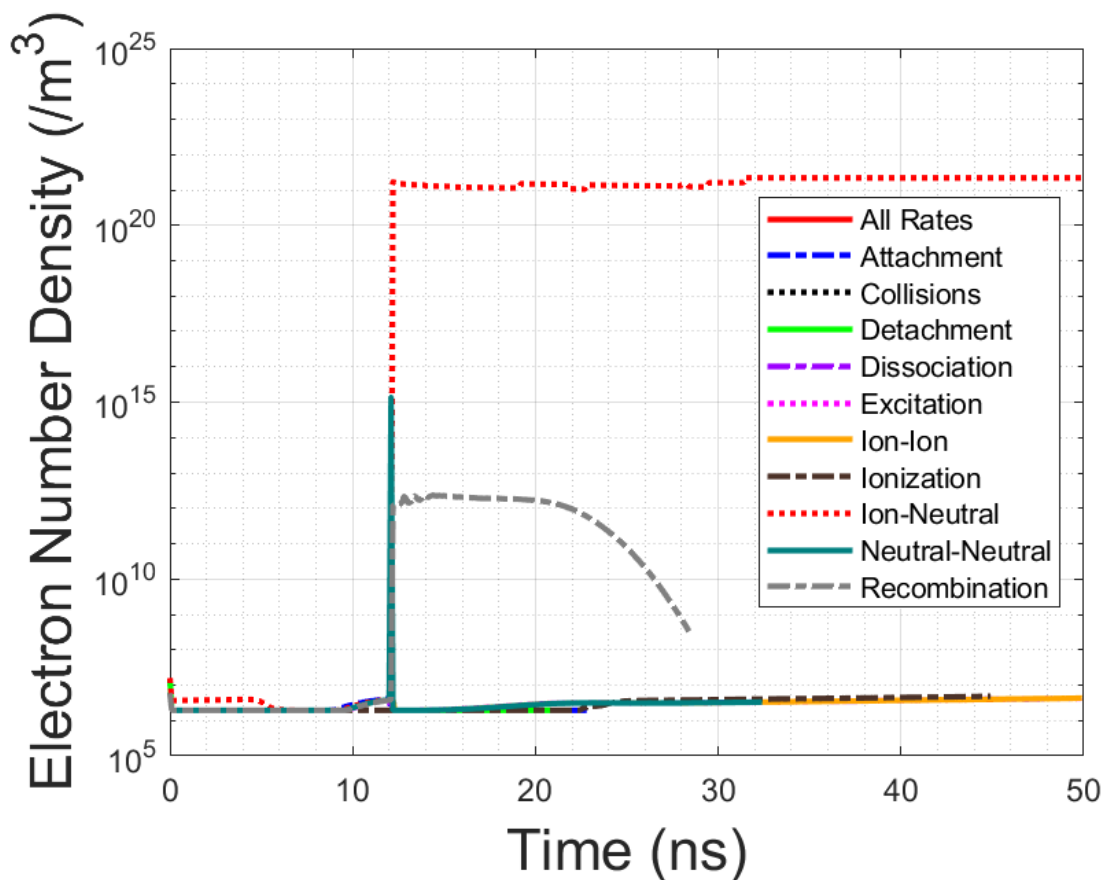


Figure 3.10: Effects of Removing Categories of Reactions - Electron Density

Each curve shows the values predicted if all rates are considered EXCEPT for the one reaction by which it is named

same time that the electron temperature spikes as presented in Figure 3.6 and Figure 3.8, and it suggests that a high volume of electrons is not the only reason that impossible temperatures are being reached in the solver. This seems to suggest that a lack of reactions at high activation energies is the problem and that scCO<sub>2</sub> can see higher energies than at STP.

Surprisingly, removing excitation reactions does not deviate the results much from a simulation including all 176 reactions. At first glance, this may seem to conflict with Figure 3.7, but this study did not differentiate between the types of excitation, such as electronic vs. vibrational. Additionally, there is still the possibility of not including enough excitation reactions to cover the range of activation energy that would be expected in scCO<sub>2</sub>.

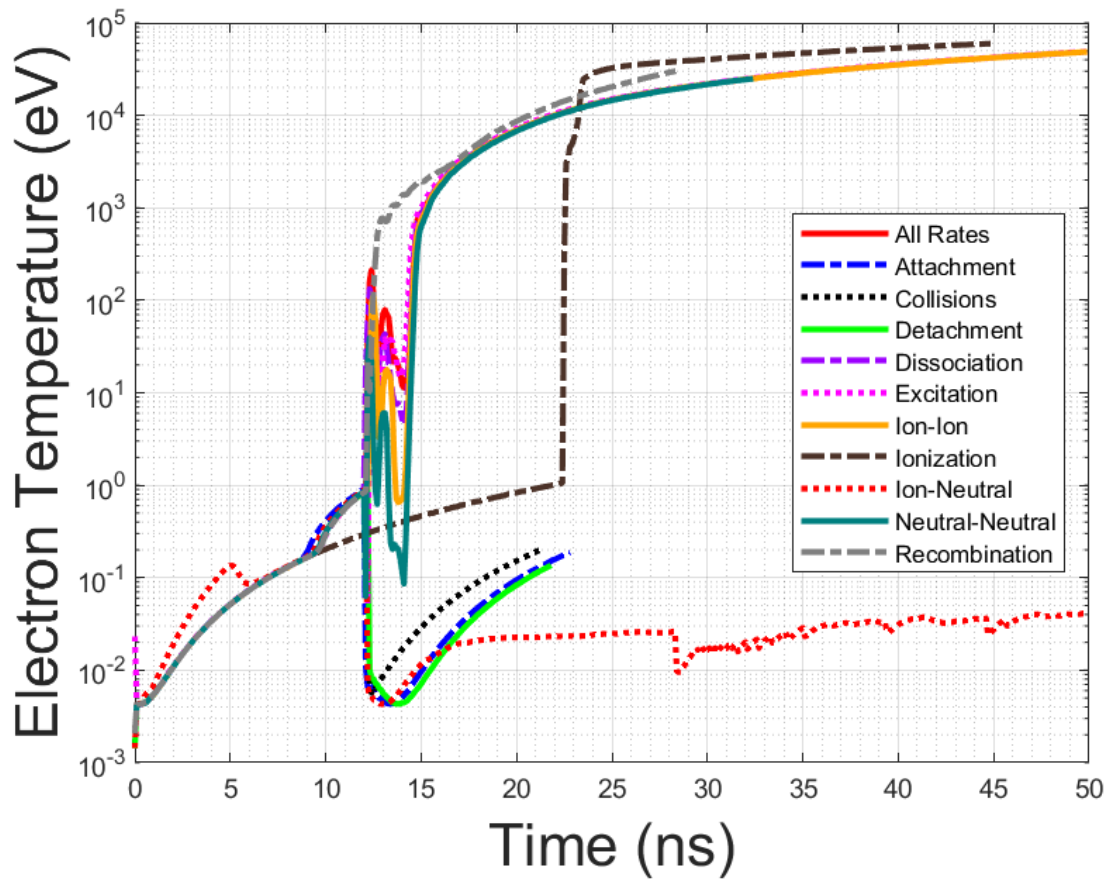


Figure 3.11: Effects of Removing Categories of Reactions - Electron Temperature

Each curve shows the values predicted if all rates are considered EXCEPT for the one reaction by which it is named

## CHAPTER 4

### RESULTS - NOZZLE

The nozzle geometry was investigated to understand the effects of geometry and more realistic distances between the contacts. Similar to the parallel plates case, the nozzle was run in a series of parametric tests, to include the study of scCO<sub>2</sub> densities.

#### 4.1 Mesh Sensitivity Study

The first tests run were a mesh sensitivity study at STP with an initial electron density of  $1e10$  and a current source of 10 A. Another thing to note is the gap distance is 15 mm rather than 10 mm, for no particular reason. The results for 0.005, 0.004, 0.003, and 0.002 m cell sizes are shown in Figure 4.1.

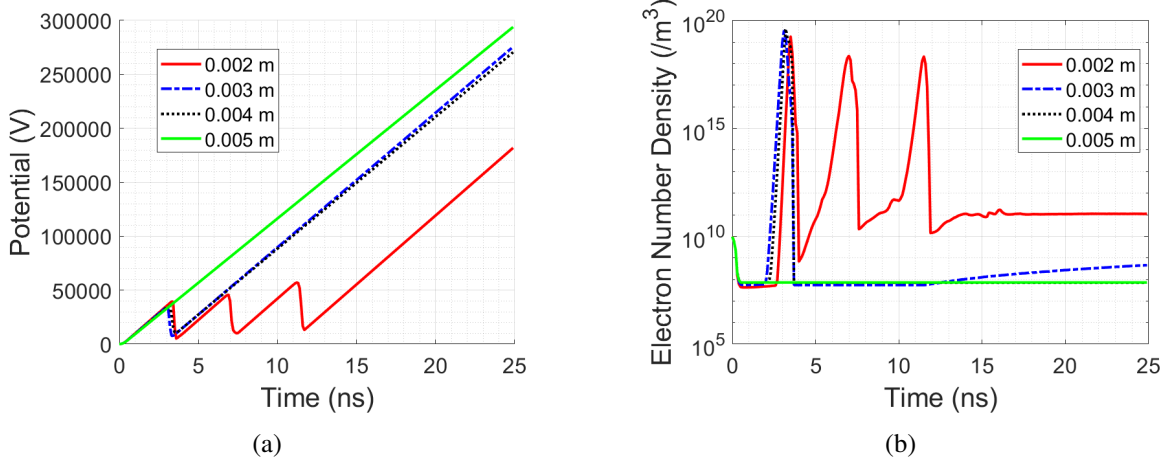


Figure 4.1: Mesh Sensitivity Study

Similar to the parallel plates case, the most fine mesh displays unexpected behavior compared to the coarser cases. Additionally, the most coarse case shows almost no change in the simulation, suggesting that 0.005 m is too coarse to capture interactions between particles.

The middle two cases, 0.003 and 0.004 m, show almost identical behavior in potential and electron number density. The 0.002 m case deviates from this behavior, and the areas of high electron density in the nozzle may explain this deviation. When the first temporary breakdown occurs, this happens right at the contact, as expected, for each of the mesh sizes. This is shown in Figure 4.2.

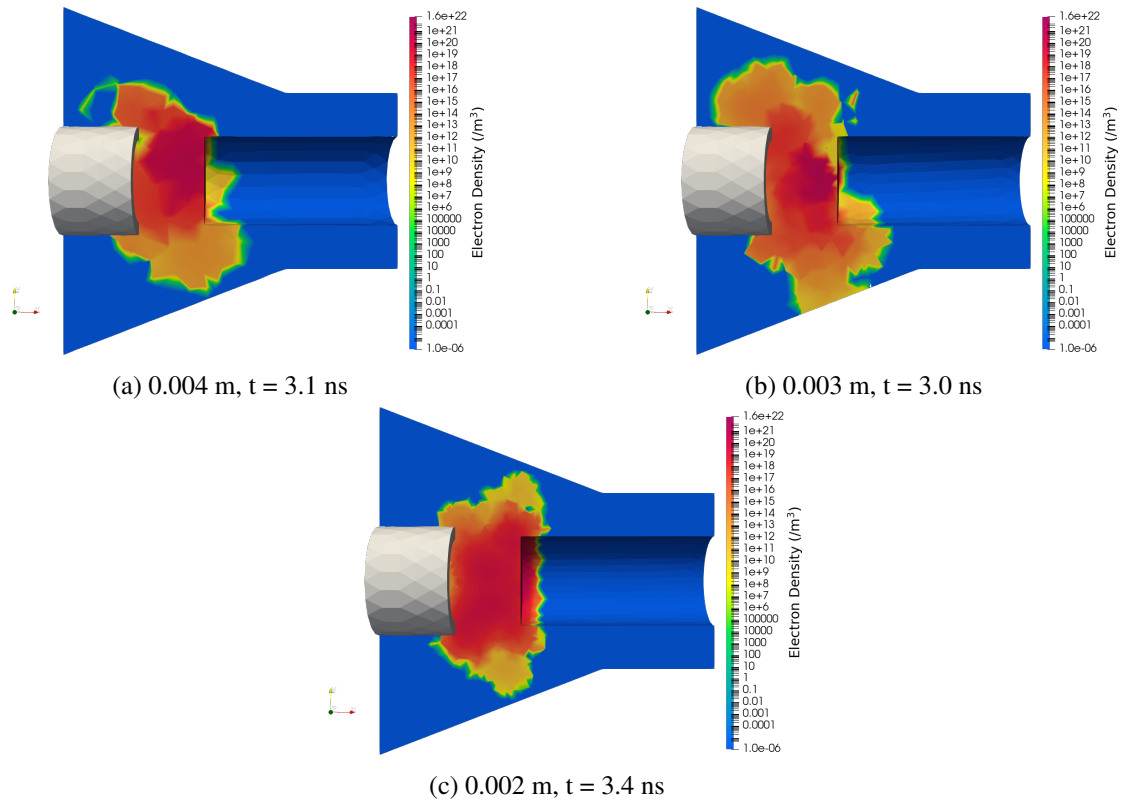


Figure 4.2: Comparison of Breakdown Across Meshes

Breakdown does not happen again for either of the cases, but for the 0.002 m mesh, spots of high electron density happen in unexpected areas in the nozzle. This is shown in Figure 4.3.

While there is still a concentration of electrons around the anode, this is not where the spike in electron density happens. Rather, it is seen in other areas of the nozzle, which contribute to a higher electron density over the whole domain. The results seem to suggest that ionization is happening away from the anode in the 0.002 m case, and this may require further study to see if an even finer mesh is required to capture these interactions in the

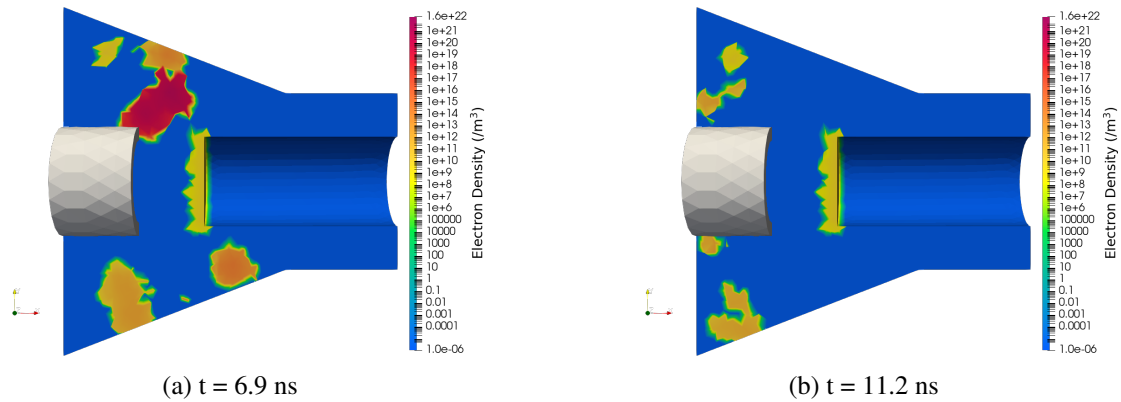


Figure 4.3: Additional Spikes in Electron Density

lower energy areas of the nozzle. Additionally, if this phenomenon continues occurring, the way potential is extracted from the simulation may also require adjustment. While each spike in electron density correlated to a potential breakdown, visually, the breakdown that is expected in a circuit breaker is not happening. The assumption is that the potential difference is happening between the anode body of 0 V and the cathode of some non-zero voltage, but in the two cases of Figure 4.3, this potential might be calculating incorrectly because of the electron densities occurring away from the contact.

While the potential might require some adjustment in this case, these two cases of electron formation present an interesting point of study. At face value, these results seem to indicate that, after the initial breakdown, there is enough energy remaining in the nozzle to create more electrons in the fluid away from the contacts, but there are not enough to cause another breakdown. Additionally, this formation of electrons happens again, but the areas are much smaller, suggesting the system continuously loses energy and the ability to produce electrons. Further investigation into this phenomenon is required as well as a more detailed mesh sensitivity test, but for the purposes of this study, 0.004 m was the final mesh chosen in order to avoid possible interference in results from electron production away from the contacts.

## 4.2 scCO<sub>2</sub>

The initial electron density determined from the parallel plates simulation was  $1.75e7$  electrons, but initial results from scCO<sub>2</sub> did not breakdown in these conditions, even when increasing the current source to force a higher potential. It is possible that a jump of 10 mm in a static simulation is too far for an arc to strike in scCO<sub>2</sub> in these conditions, so the initial electron density was artificially increased in an attempt to determine what electron density is required to see breakdown in the simulation.

### 4.2.1 Investigation of Contact Distances

In a gap study operating at scCO<sub>2</sub> conditions, the system was still unable to breakdown. This may not necessarily be a surprising result, given the high density of scCO<sub>2</sub>, but as before, numerical heating could create some concern. The results are shown in Figure 4.4.

The potential raises some questions, as increasing the max current source value should be the only parameter that changes the rate at which the potential builds. Regardless, breakdown does not happen at all, even as the potential climbs to infinity. However, further investigation of the electron temperature further confirms that instability in the electron temperature is still an issue at higher densities. To confirm where numerical heating seems to occur, a couple more tests were conducted. The first was done at STP conditions with 138 reactions. The second was done with a functioning N<sub>2</sub> library provided with the program.

Figure 4.5 shows the results of a gap distance study when returning to the original set of 138 reactions at STP conditions.

As expected, the larger the gap distance is, the larger the breakdown potential becomes, though the rate of increase in the potential still shows an unexpected dependency on gap distance. The critical electron density increases from 1 mm to 15 mm, which also makes sense. The critical electron density for 15 mm is estimated to be  $2.62e18 \text{ m}^{-3}$ , which is an

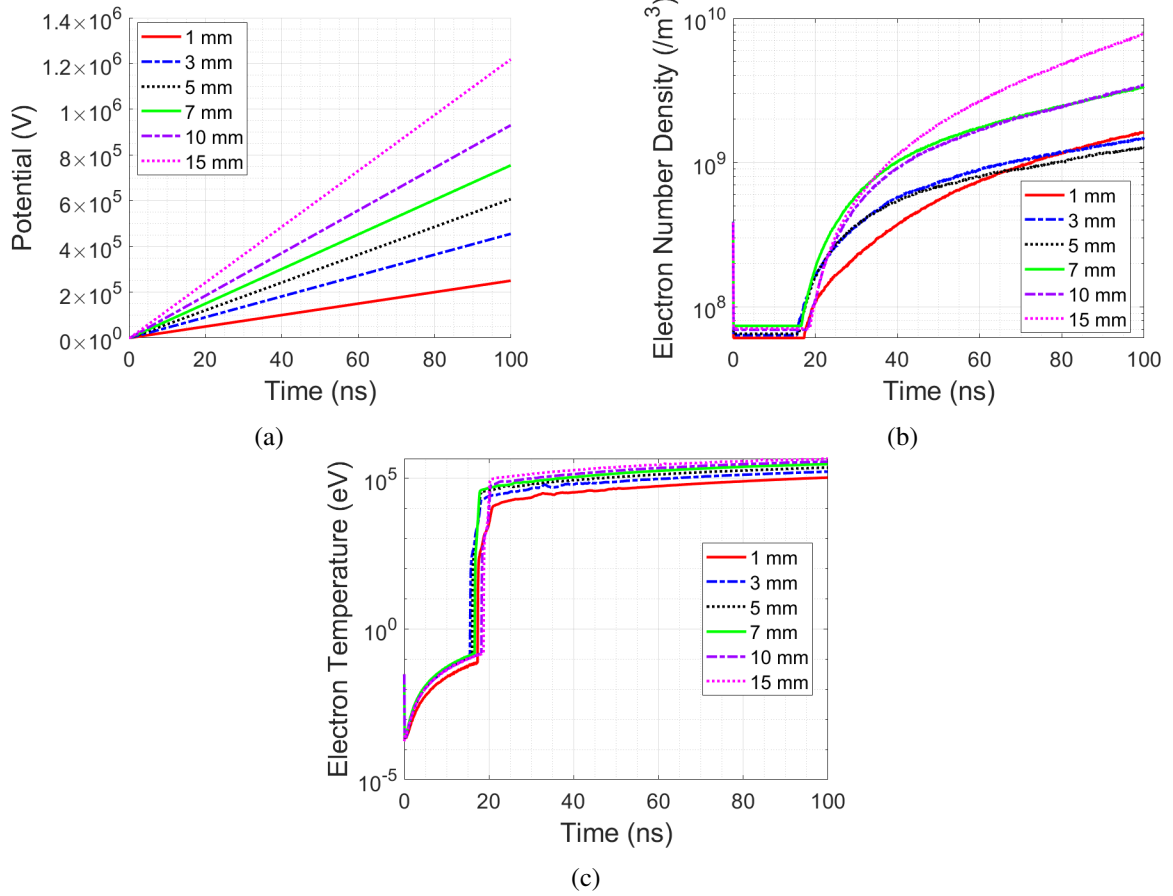


Figure 4.4: Investigation of Contact Distances -  $\text{scCO}_2$

order of magnitude larger than the critical electron density at 1 mm,  $6.4102 \times 10^{16} \text{ m}^{-3}$ . The same trends can be seen in  $\text{N}_2$ , shown in Figure 4.6.

Interestingly,  $\text{N}_2$  takes longer to breakdown than  $\text{CO}_2$ . This could indicate slower reaction rates or less ionization rates, but it takes significantly less electrons to breakdown. Compared to  $2.62 \times 10^{18} \text{ m}^{-3}$  in  $\text{CO}_2$ ,  $\text{N}_2$  becomes conductive at  $9.80 \times 10^{16} \text{ m}^{-3}$ .

### 4.3 Reaction Studies

Similar to the parallel plates case, only the omission of a couple types of reactions have an obvious effect on the simulation. These cases were run at  $1.75 \times 10^7$  initial electron density, a gap distance of 15 mm, and a current source of 10 A at supercritical conditions. As seen in Figure 4.7, most of the cases do not see any type of breakdown over the simulation, but re-

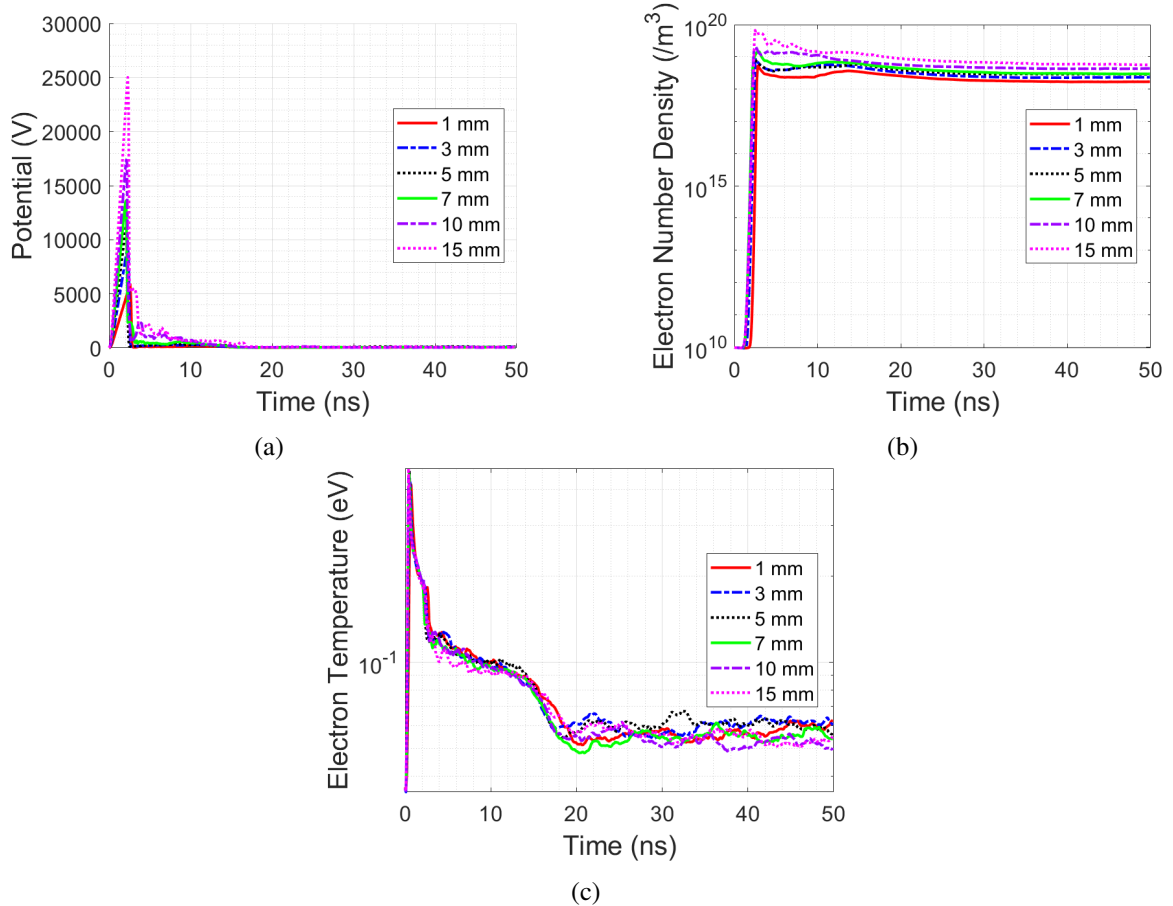


Figure 4.5: Investigation of Contact Distances - STP  $CO_2$  (138 Reactions)

removal of ion-neutral reactions and recombination reactions cause some type of breakdown, even if it is comparably small.

Similar to the plates case, ion-neutral reactions seem to play a significant role in removing energy from the system that prevent breakdown. Again, this may be indicative of a disproportionate emphasis on ion-neutral type reactions. The other interesting behavior from removing ion-neutral reactions is the resultant sawtooth pattern, similar to the behavior found in the mesh sensitivity study. This is also reflected in Figure 4.8 and Figure 4.9.

In Figure 4.9, the sawtooth trend actually stays within reasonable electron temperature bounds. This has an interesting correlation to Figure 4.1b. At around 18 ns, the electron temperature does reach nonphysical values, but this corresponds to a sharp drop in electrons that stays constant around  $1e9$  for the rest of the simulation. This may also be explained

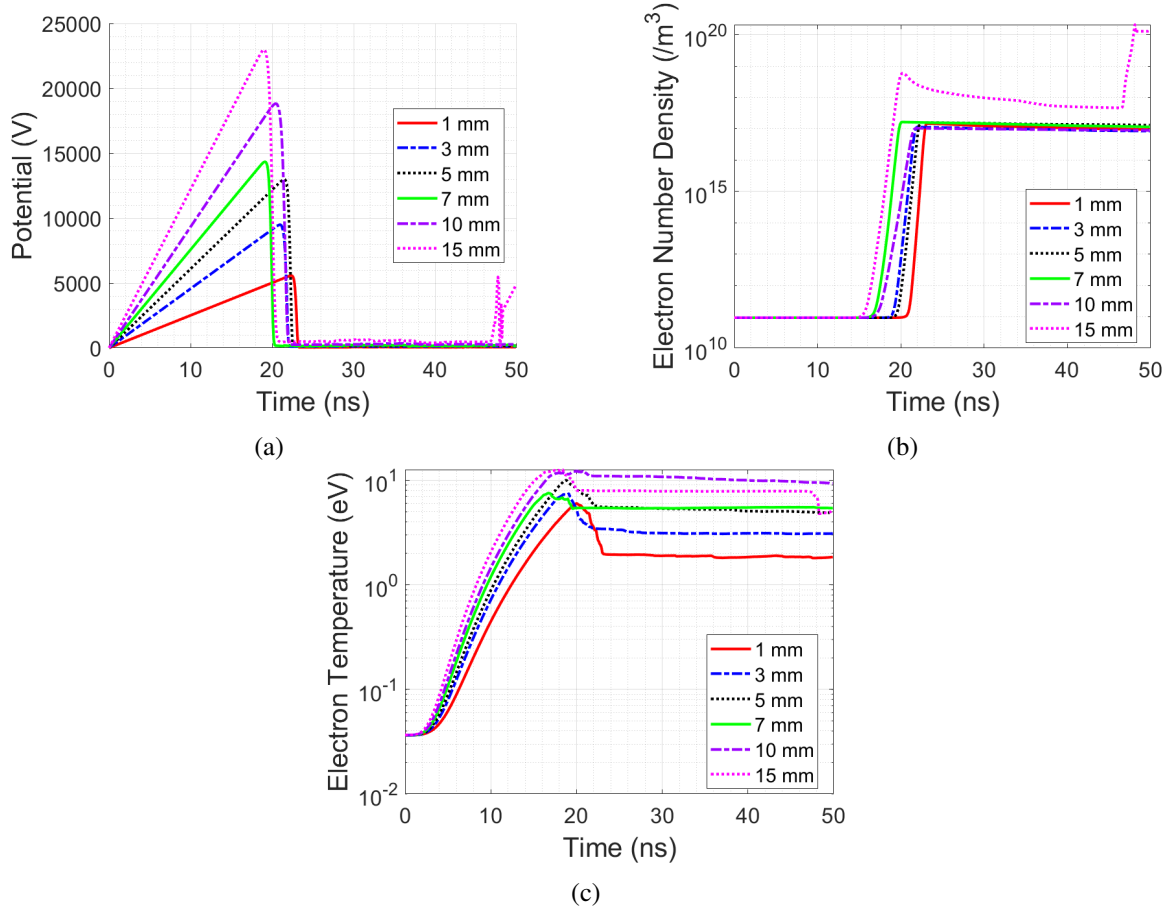


Figure 4.6: Investigation of Contact Distances -  $N_2$

by the lack of functioning inlets and outlets, as the solver tries to maintain a certain density once the electron temperature reaches values outside of the range of reactions included.

An additional look at the sawtooth behavior might be reminiscent of the phenomenon that occurred during the mesh sensitivity study, but a visual inspection of the PIC results in Figure 4.10 show that what is happening here is different.

The last interesting thing to note is that recombination, despite having an effect on the potential, does not have too much of an effect on electron temperature or density; therefore, the small dip in potential might be negligible. On the other hand, omitting ionization has a more obvious effect on electron density and electron temperature that is not as obvious in the potential. Just like in the parallel plates case, omitting ionization delays the point where electrons start being produced in the system. Once electrons start being produced,

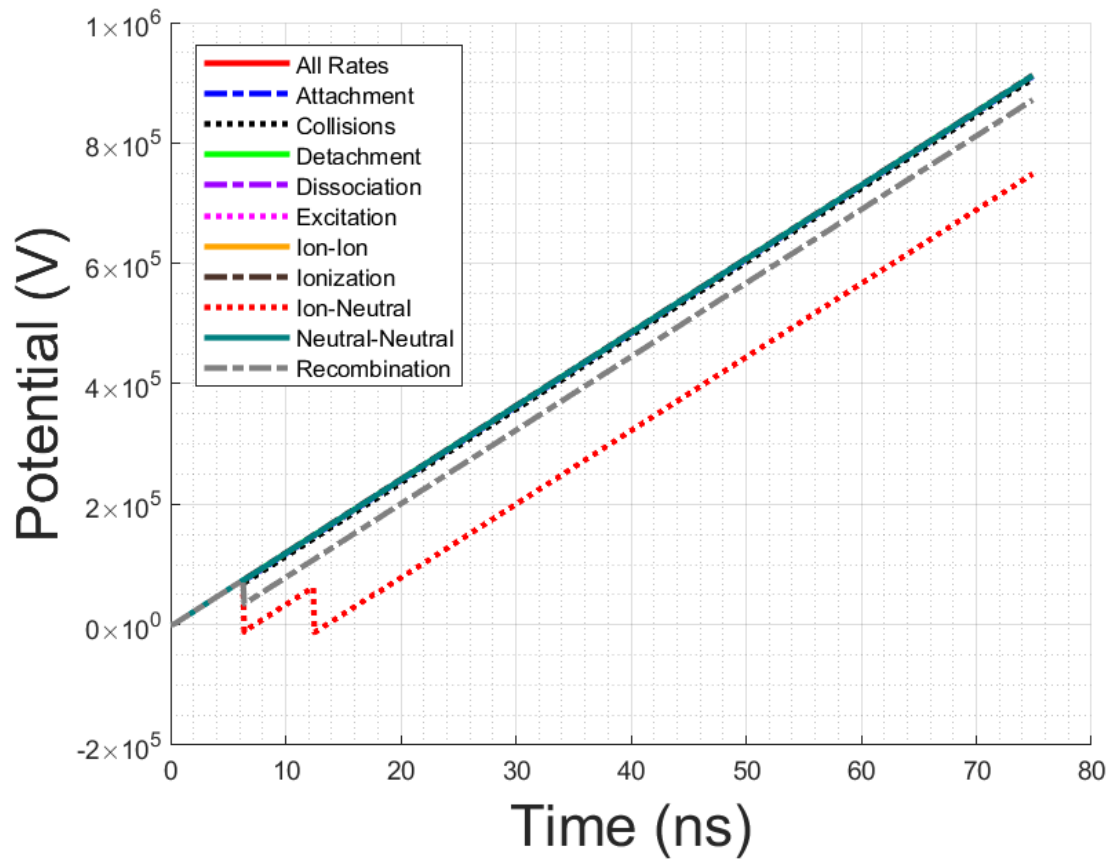


Figure 4.7: Effects of Removing Categories of Reactions - Potential

the electron temperature spikes as normal, further linking the production of electrons to producing nonphysical electron temperature values.

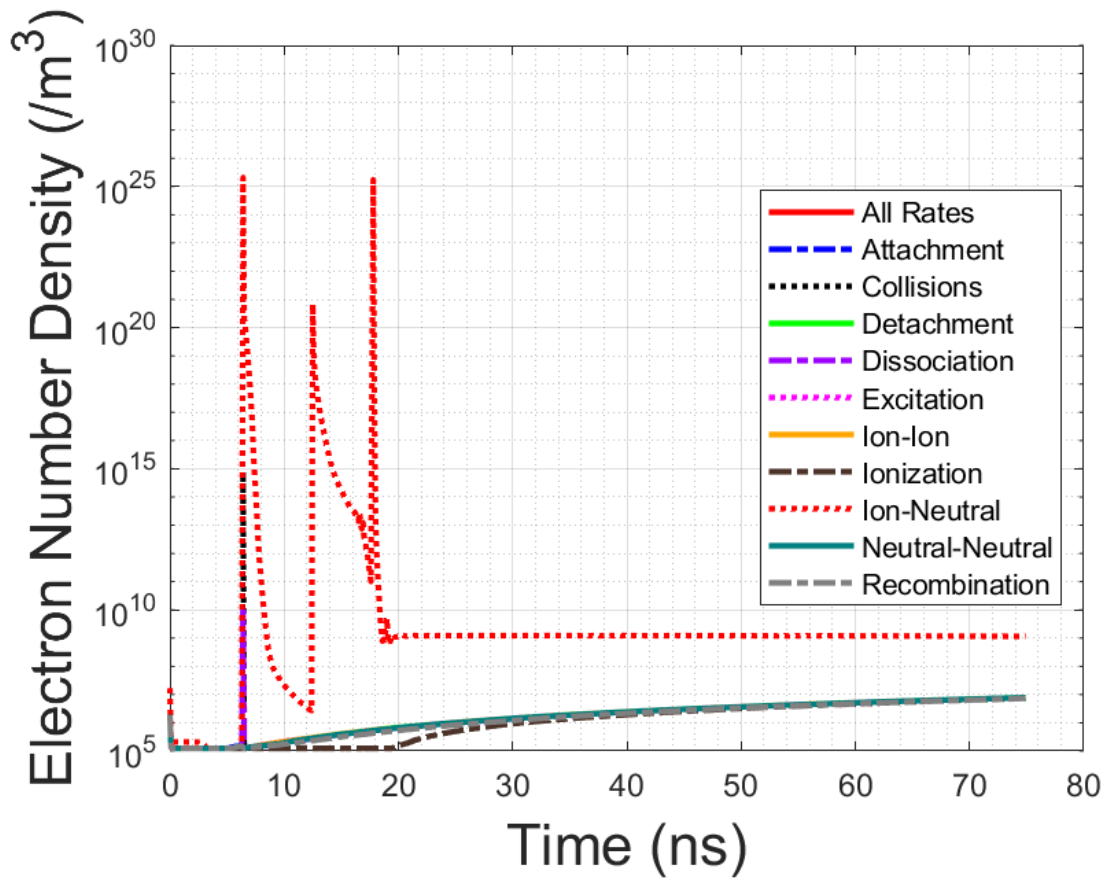


Figure 4.8: Effects of Removing Categories of Reactions - Electron Density

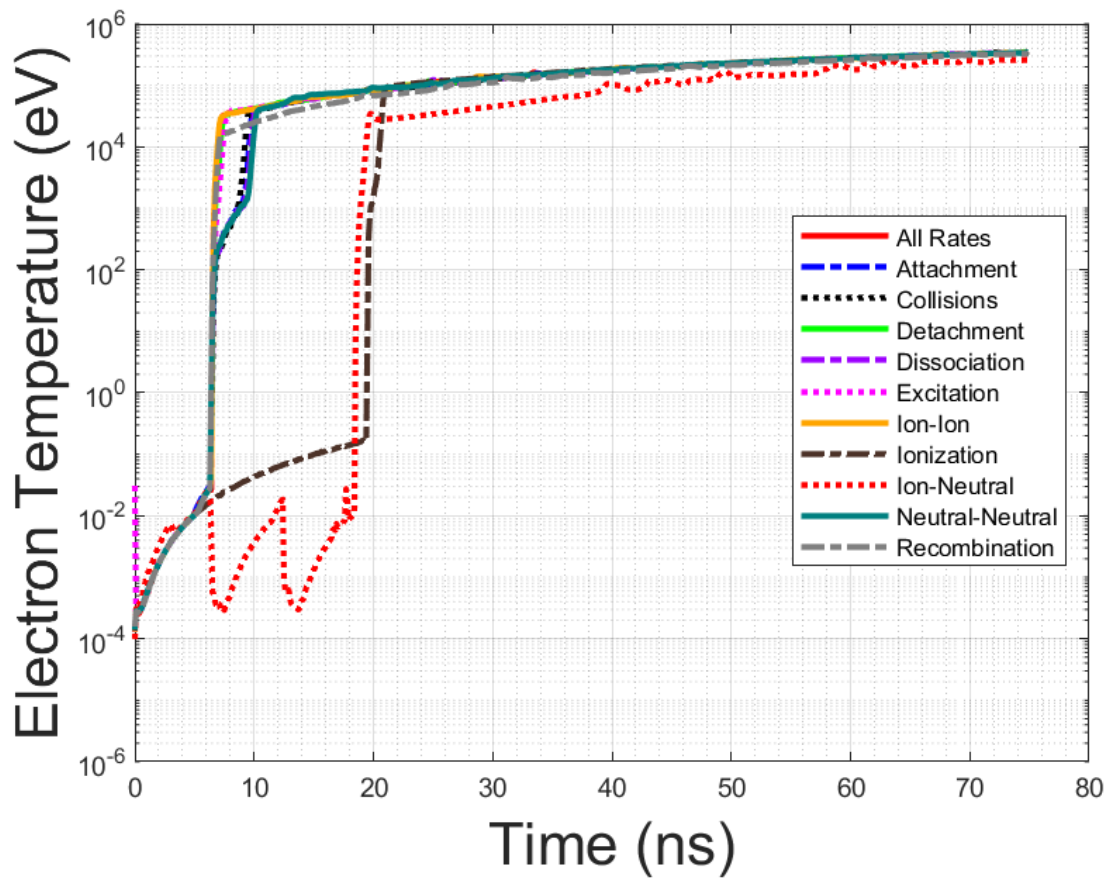


Figure 4.9: Effects of Removing Categories of Reactions - Electron Temperature

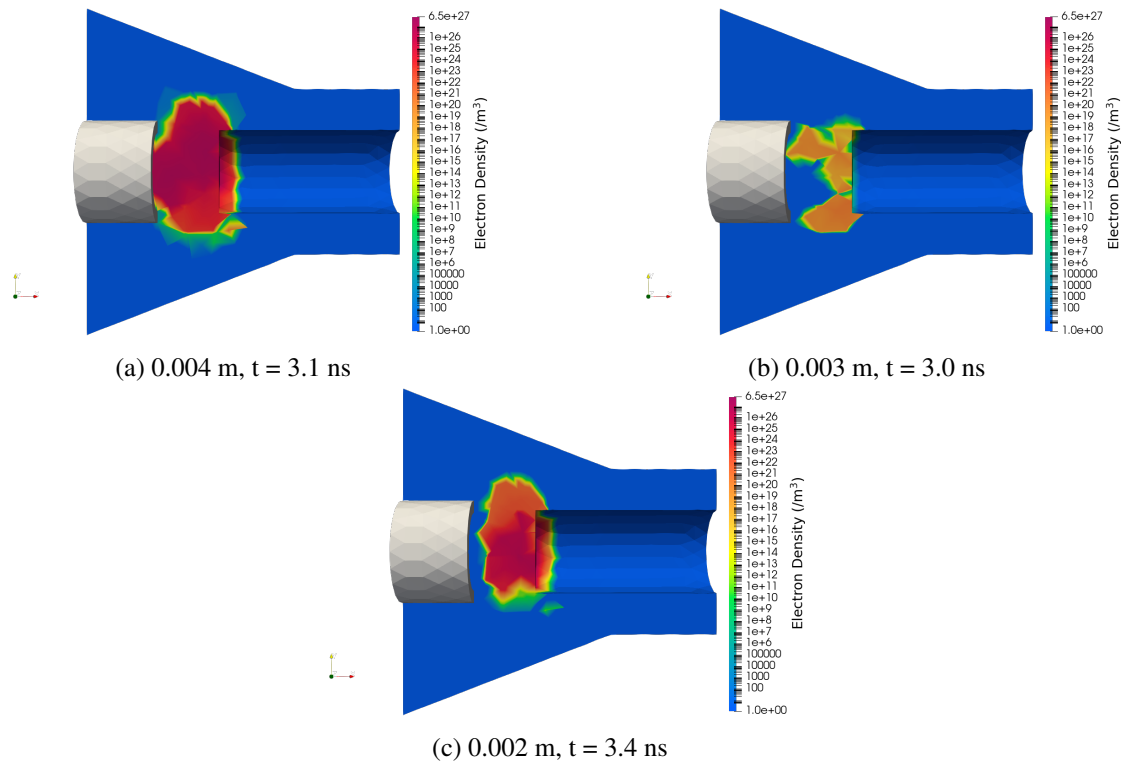


Figure 4.10: Comparison of Breakdown Across Meshes

## CHAPTER 5

### DISCUSSION

#### 5.1 Future Work

##### 5.1.1 Model Improvements

There is still room for improvement on the presented model, and there are a number of factors that need to be addressed further. Some of the critical improvements include:

1. Numerical Instabilities
2. Reactions
3. Particle Inlets and Outlets

Addressing the reactions provided to the solver will be the longest and most difficult factor to get right, but it will also be the most important. There is little to no literature or work investigating a set of reactions to describe the behavior of  $\text{CO}_2$  at such high pressures, though there are some sets to work off of for  $\text{CO}_2$  at STP. As found in this work, the set of reactions for  $\text{scCO}_2$  becomes unstable after the initial breakdown, reaching nonphysical electron temperatures. One of the reasons for this spike seems to be an inadequate amount of higher-energy reactions, suggesting that  $\text{scCO}_2$  gains much more energy than  $\text{CO}_2$ . Another reason could be numerical instabilities native to the solver that will have to be addressed from the developer side. Either way, whatever factor is causing the electron temperature to grow unbounded will have to be isolated and fixed.

Second, the set of reactions provided for STP  $\text{CO}_2$  do not seem to be sufficient to describe  $\text{scCO}_2$ . Based on [16] and other literature, there may need to be an emphasis on types of excitation reactions (electronic, vibrational, etc.) as well as covering a larger range of activation energies. Additionally,  $\text{scCO}_2$  has a short mean free path, which would lead to

energy loss through collisions, but initial results showed that only ion-neutral reactions had a large impact on the solver. Including more neutral-neutral reactions, for example, might help reflect the expected behavior of a fluid with a short mean free path.

Finally, the inclusion of particle inlets and outlets is an important factor to update to more closely resemble the real physics of a circuit breaker, but this factor is dependent on the development of the program. Once inlets and outlets are implemented, this will allow the simulation to specify loss surfaces where electrons can flow out of the computational space. For the simulations outlined in this work, specifically in the nozzle case, electrons are not necessarily forced to exit through one of the contacts, and this could be leading to random clumps of electrons, as seen in the finest nozzle mesh case. While the development team works towards moving geometry, outlets will be necessary to accurately recreate the shape of an arc strike in simulation with static contacts.

These improvements should help increase the model's accuracy. To better fit the model to TESLA's problem, there are several more factors to adjust. First, the current source should be adjusted to match the worst case scenario of the actual circuit breaker. This information could be simple to find in literature or through small-scale experiments since the current source and the voltage source in an actual electrical circuit are related. Second, field and thermionic emissions should be included to help eliminate uncertainty from the initial electron density. It would be expected for thermionic emission to dominate electron production, so the addition of this factor into the simulation will help determine whether  $\text{scCO}_2$  can prevent restrike with high electron emissions and under what conditions.

### 5.1.2 Topics of Interest

The results from this work also introduce many relevant questions that should be further investigated. The first is the question of the mesh size and time step. While the initial recommendations for STP were assumed to hold true at supercritical pressures, it cannot be stated conclusively if this is a good assumption yet. If the time step and mesh size are not

small enough, a significant amount of particle interaction and movement may be omitted from the final results.

Another topic of interest includes the inclusion of oxygen in the system.  $\text{scCO}_2$  lacks the electronegativity required to absorb excess electrons after the initial arc quench to the same degree as  $\text{SF}_6$ , but oxygen may be able to fill this role through attachment. While this is not a point of focus for this work and also is not heavily represented in the reactions list, it may be worth investigating the role of  $\text{O}_2$  in preventing restrike.

## 5.2 Further Application to Relevant Fields

The concept of molecular kinetics is not one that is just limited to supercritical  $\text{CO}_2$  or industrial circuit breakers. EMA3D® advertises Ansys Charge Plus as being applicable to space environments as well, specifically surface charging due to triboelectrification and low- or high- energy plasma environments. It also has the ability to do internal charging of a solid material, lending to material studies of vehicles in space environments. This method also holds relevance to hypersonic flows and vehicles, which is another large topic of interest recently.

Hypersonics is a field of research that largely has to consider problems such as non-equilibrium, and these hypersonic vehicles often operate outside of atmospheric conditions. Some works already see the potential in particle-based simulations when used in application to hypersonics, with some that use the Monte-Carlo Method utilized by Ansys Charge Plus[18, 19, 20] and others that use different computational methods to determine the position of a particle after a time step[21]. One study even compares the effectiveness of different methods in estimating shock structures[22], and concluded that the Monte-Carlo results were in excellent agreement with experimental results. With the steadily increasing complexity of aerospace problems, particle-based, non-equilibrium solver methods stand to provide answers that are not readily available with conventional continuum based fluid dynamics in fields such as space travel and hypersonics, or any propulsion concept or vehicle

operating in rarefied gases.

## CHAPTER 6

### CONCLUSION

Significant steps have been taken towards understanding the phenomenon of arc restrike in  $\text{scCO}_2$ . From initial results,  $\text{scCO}_2$  looks to have great potential in preventing arc restrike, but there is still limited confidence in the simulation's accuracy. Challenges such as numerical instabilities in the electron temperature or in the reaction lists have a non-negligible effect on results, though it is still unsure as to what extent. An interesting conclusion to draw from the simulations is that ion-neutral reactions dominated energy loss. Even if  $\text{scCO}_2$  does not have as much electronegativity as  $\text{SF}_6$ , there is still the possibility of high energy losses from ion and neutral collisions, though a more in-depth reaction list study would have to be done to state this conclusively.

Charge Plus proves to be a promising tool, and with the fixes proposed by this work, a working model for arc reignition in  $\text{scCO}_2$  is well underway. The most pressing fix to address first would be the instabilities that seem to be present in the electron temperatures. In addition to this, there are other developments underway for Charge Plus that will help improve further iterations of the models. Unfortunately, the simulations are difficult to validate for  $\text{scCO}_2$ , because measurements do not exist for this medium at high pressures as needed for this modeling effort. Most important will be understanding the number of electrons emitted from the contacts due to field or thermionic emission effects. This could be done parametrically to determine how many emitted electrons  $\text{scCO}_2$  can diffuse without restrike, similar to the initial density tests, but experimental or computational validation could help narrow these guesses of emitted electrons.

# **Appendices**

**APPENDIX A**  
**FULL LIST OF REACTIONS ORDERED BY TYPE**

Table A.1: Cross-sectional Collision Reactions

<b>Reaction<sup>1</sup></b>	<b>Rate Coefficients <math>m^3/s</math></b>	<b>Reference<sup>2</sup></b>
<b>Elastic</b>		
$e^- + CO_2 \rightarrow e^- + CO_2^+ + 0eV$	Cross-Section	[15]
$e^- + CO \rightarrow e^- + CO + 0eV^*$	Cross-Section	[15, 23]
$e^- + C \rightarrow e^- + C + 0eV^*$	Cross-Section	[15, 24]
<b>Excitation</b>		
$e^- + C \rightarrow e^- + C + 1.302eV$	Cross-Section	LXCAT
$e^- + C \rightarrow e^- + C + 2.629eV$	Cross-Section	LXCAT
$e^- + C \rightarrow e^- + C + 3.963eV$	Cross-Section	LXCAT
$e^- + C \rightarrow e^- + C + 7.527eV$	Cross-Section	LXCAT
$e^- + C \rightarrow e^- + C + 7.5eV$	Cross-Section	LXCAT
$e^- + C \rightarrow e^- + C + 8.004eV$	Cross-Section	LXCAT
$e^- + C \rightarrow e^- + C + 8.534eV$	Cross-Section	LXCAT
$e^- + C \rightarrow e^- + C + 8.649eV$	Cross-Section	LXCAT
$e^- + C \rightarrow e^- + C + 8.775eV$	Cross-Section	LXCAT
$e^- + C \rightarrow e^- + C + 8.857eV$	Cross-Section	LXCAT
$e^- + C \rightarrow e^- + C + 9.014eV$	Cross-Section	LXCAT
$e^- + C \rightarrow e^- + C + 9.172eV$	Cross-Section	LXCAT
$e^- + C \rightarrow e^- + C + 9.379eV$	Cross-Section	LXCAT

<sup>1</sup>\* indicates an addition made to original set provided by eMA3D®

<sup>2</sup>empty indicates unknown origin of reaction

Table A.1: Continued

$e^- + C \rightarrow e^- + C + 9.614eV$	Cross-Section	LXCAT
$e^- + C \rightarrow e^- + C + 9.673eV$	Cross-Section	LXCAT
$e^- + C \rightarrow e^- + C + 9.685eV$	Cross-Section	LXCAT
$e^- + C \rightarrow e^- + C + 9.687eV$	Cross-Section	LXCAT
$e^- + C \rightarrow e^- + C + 9.705eV$	Cross-Section	LXCAT
$e^- + C \rightarrow e^- + C + 9.716eV$	Cross-Section	LXCAT
$e^- + C \rightarrow e^- + C + 9.748eV$	Cross-Section	LXCAT
$e^- + C \rightarrow e^- + C + 9.84eV$	Cross-Section	LXCAT
$e^- + CO \rightarrow e^- + CO + 6.006eV$	Cross-Section	LXCAT
$e^- + CO \rightarrow e^- + CO + 6.863eV$	Cross-Section	LXCAT
$e^- + CO \rightarrow e^- + CO + 8.024eV$	Cross-Section	LXCAT
$e^- + CO \rightarrow e^- + CO + 10.399eV$	Cross-Section	LXCAT
$e^- + CO \rightarrow e^- + CO + 10.777eV$	Cross-Section	LXCAT
$e^- + CO \rightarrow e^- + CO + 11.396eV$	Cross-Section	LXCAT
$e^- + CO \rightarrow e^- + CO + 11.524eV$	Cross-Section	LXCAT
$e^- + CO \rightarrow e^- + CO + 2.58eV^*$	Cross-Section	[23]
$e^- + CO \rightarrow e^- + CO + 2.33eV^*$	Cross-Section	[23]
$e^- + CO \rightarrow e^- + CO + 2.09eV^*$	Cross-Section	[23]
$e^- + CO \rightarrow e^- + CO + 1.84eV^*$	Cross-Section	[23]
$e^- + CO \rightarrow e^- + CO + 1.59eV^*$	Cross-Section	[23]
$e^- + CO \rightarrow e^- + CO + 1.33eV^*$	Cross-Section	[23]
$e^- + CO \rightarrow e^- + CO + 1.07eV^*$	Cross-Section	[23]
$e^- + CO \rightarrow e^- + CO + 0.266eV^*$	Cross-Section	[23]
$e^- + CO \rightarrow e^- + CO + 0.81eV^*$	Cross-Section	[23]

Table A.1: Continued

$e^- + CO \rightarrow e^- + CO + 0.54eV^*$	Cross-Section	[23]
$e^- + CO_2 \rightarrow e^- + CO_2 + 9eV$	Cross-Section	LXCAT
$e^- + CO_2 \rightarrow e^- + CO_2 + 11eV$	Cross-Section	LXCAT
$e^- + CO_2 \rightarrow e^- + CO_2 + 18.1eV^*$	Cross-Section	[25]
$e^- + CO_2 \rightarrow e^- + CO_2 + 17.3eV^*$	Cross-Section	[25]
$e^- + CO_2 \rightarrow e^- + CO_2 + 12.4eV^*$	Cross-Section	[25]
$e^- + CO_2 \rightarrow e^- + CO_2 + 11.9eV^*$	Cross-Section	[25]
$e^- + CO_2 \rightarrow e^- + CO_2 + 10.5eV^*$	Cross-Section	[23]
$e^- + CO_2 \rightarrow e^- + CO_2 + 7.0eV^*$	Cross-Section	[23]
$e^- + CO_2 \rightarrow e^- + CO_2 + 5.7eV^*$	Cross-Section	[26]
$e^- + CO_2 \rightarrow e^- + CO_2 + 2.5eV^*$	Cross-Section	[26]
$e^- + CO_2 \rightarrow e^- + CO_2 + 0.505eV^*$	Cross-Section	[23]
$e^- + CO_2 \rightarrow e^- + CO_2 + 0.422eV^*$	Cross-Section	[23]
$e^- + CO_2 \rightarrow e^- + CO_2 + 0.339eV^*$	Cross-Section	[23]
$e^- + CO_2 \rightarrow e^- + CO_2 + 0.291eV^*$	Cross-Section	[26]
$e^- + CO_2 \rightarrow e^- + CO_2 + 0.252eV^*$	Cross-Section	[23]
$e^- + CO_2 \rightarrow e^- + CO_2 + 0.172eV^*$	Cross-Section	[26]
$e^- + CO_2 \rightarrow e^- + CO_2 + 0.167eV^*$	Cross-Section	[23]
$e^- + CO_2 \rightarrow e^- + CO_2 + 0.083eV^*$	Cross-Section	[26]
$e^- + CO_2 \rightarrow e^- + CO_2 + 0.36eV^*$	Cross-Section	[26]
$e^- + CO_2 \rightarrow e^- + CO_2 + 0.5eV^*$	Cross-Section	[23]
$e^- + O \rightarrow e^- + O + 1.967eV$	Cross-Section	LXCAT
$e^- + O \rightarrow e^- + O + 4.19eV$	Cross-Section	LXCAT
$e^- + O \rightarrow e^- + O + 9.146eV$	Cross-Section	LXCAT

Table A.1: Continued

$e^- + O \rightarrow e^- + O + 9.521eV$	Cross-Section	LXCAT
$e^- + O \rightarrow e^- + O + 10.74eV$	Cross-Section	LXCAT
$e^- + O \rightarrow e^- + O + 10.99eV$	Cross-Section	LXCAT
$e^- + O \rightarrow e^- + O + 12.09eV$	Cross-Section	LXCAT
$e^- + O \rightarrow e^- + O + 12.54eV$	Cross-Section	LXCAT
$e^- + O \rightarrow e^- + O + 13eV$	Cross-Section	LXCAT
$e^- + O \rightarrow e^- + O + 14.12eV$	Cross-Section	LXCAT
$e^- + O \rightarrow e^- + O + 15.66eV$	Cross-Section	LXCAT
$e^- + O \rightarrow e^- + O + 16.11eV$	Cross-Section	LXCAT
$e^- + O_2 \rightarrow e^- + O_2 + 0.977eV$	Cross-Section	LXCAT
$e^- + O_2 \rightarrow e^- + O_2 + 1.627eV$	Cross-Section	LXCAT
$e^- + O_2 \rightarrow e^- + O_2 + 4.5eV$	Cross-Section	LXCAT
$e^- + O_2 \rightarrow e^- + O_2 + 9.3eV$	Cross-Section	LXCAT
$e^- + O_2 \rightarrow e^- + O_2 + 14.7eV^*$	Cross-Section	[23]
$e^- + O_2 \rightarrow e^- + O_2 + 9.97eV^*$	Cross-Section	[23]
$e^- + O_2 \rightarrow e^- + O_2 + 8.4eV^*$	Cross-Section	[23]
$e^- + O_2 \rightarrow e^- + O_2 + 6.0eV^*$	Cross-Section	[23]
$e^- + O_2 \rightarrow e^- + O_2 + 0.38eV^*$	Cross-Section	[23]
$e^- + O_2 \rightarrow e^- + O_2 + 0.19eV^*$	Cross-Section	[23]
$e^- + O_2 \rightarrow e^- + O_2 + 0.8eV^*$	Cross-Section	[23]
$e^- + O_2 \rightarrow e^- + O_2 + 0.6eV^*$	Cross-Section	[23]
<b>Dissociation</b>		
$e^- + CO \rightarrow e^- + C + O + 11.1eV$	Cross-Section	[14]
$e^- + CO_2 \rightarrow e^- + CO + O + 6.5eV$	Cross-Section	[14, 13]

Table A.1: Continued

$e^- + CO_2 \rightarrow e^- + CO + O + 6.75eV$	Cross-Section	[14, 13]
$e^- + CO_2 \rightarrow e^- + CO + O + 7eV$	Cross-Section	[14, 13]
$e^- + CO_2 \rightarrow e^- + CO + O + 7.25eV$	Cross-Section	[14, 13]
$e^- + CO_2 \rightarrow e^- + CO + O + 7.5eV$	Cross-Section	[14, 13]
$e^- + CO_2 \rightarrow e^- + CO + O + 7.75eV$	Cross-Section	[14, 13]
$e^- + CO_2 \rightarrow e^- + CO + O + 8eV$	Cross-Section	[14, 13]
$e^- + CO_2 \rightarrow e^- + CO + O + 8.25eV$	Cross-Section	[14, 13]
$e^- + CO_2 \rightarrow e^- + CO + O + 8.5eV$	Cross-Section	[14, 13]
$e^- + CO_2 \rightarrow e^- + CO + O + 8.75eV$	Cross-Section	[14, 13]
$e^- + CO_2 \rightarrow e^- + CO + O + 8.9eV$	Cross-Section	[14, 13]
$e^- + CO_2 \rightarrow e^- + CO + O + 9.15eV$	Cross-Section	[14, 13]
$e^- + CO_2 \rightarrow e^- + CO + O + 9.4eV$	Cross-Section	[14, 13]
$e^- + CO_2 \rightarrow e^- + CO + O + 9.65eV$	Cross-Section	[14, 13]
$e^- + CO_2 \rightarrow e^- + CO + O + 9.9eV$	Cross-Section	[14, 13]
$e^- + CO_2 \rightarrow e^- + CO + O + 10.15eV$	Cross-Section	[14, 13]
$e^- + O_2 \rightarrow e^- + 2O + 6.1eV$	Cross-Section	[14]
$e^- + O_2 \rightarrow e^- + 2O + 8.4eV$	Cross-Section	[14]
<b>Ionization</b>		
$e^- + C \rightarrow 2e^- + C^+ + 11.2eV$	Cross-Section	[15]
$e^- + CO \rightarrow 2e^- + CO^+ + 14.01eV$	Cross-Section	[15]
$e^- + CO_2 \rightarrow 2e^- + CO_2^+ + 13.8eV$	Cross-Section	[14, 13, 15]
$e^- + CO_2 \rightarrow 2e^- + CO + O^+ + 19.07eV$	Cross-Section	[14]
$e^- + CO_2 \rightarrow 2e^- + CO^+ + O + 19.47eV$	Cross-Section	[15]
$e^- + O \rightarrow 2e^- + O^+ + 13.6eV$	Cross-Section	[15]

Table A.1: Continued

$e^- + O_2 \rightarrow 2e^- + O_2^+ + 12.06eV$	Cross-Section	[15]
$e^- + O_2 \rightarrow 2e^- + O^+ + O + 23eV$	Cross-Section	[15]
<b>Attachment</b>		
$e^- + CO \rightarrow O^- + C + 0eV$	Cross-Section	[15]
$e^- + CO_2 \rightarrow CO + O^- + 0eV$	Cross-Section	[15]
$e^- + O_2 \rightarrow O^- + O + 0eV$	Cross-Section	[15]
$e^- + O_3 \rightarrow O^- + O_2 + 0eV$	Cross-Section	[15]
$e^- + O_3 \rightarrow O_2^- + O + 0eV$	Cross-Section	[15]
<b>Detachment</b>		
$O^- + CO \rightarrow e^- + CO_2 + 0eV$	6.5e-16	[13]
$O^- + O_2 \rightarrow e^- + O_3 + 0eV$	1e-18	[13]
$O^- + O_3 \rightarrow e^- + 2O_2 + 0eV$	6e-13	
$O + O^- \rightarrow e^- + O_2 + 0eV$	2.3e-16	[15]
$O_3^- + O_3 \rightarrow e^- + 3O_2 + 0eV$	3e-16	[15]
$O_2^- + O \rightarrow e^- + O_3 + 0eV$	1.5e-19	
$O_3^- + O \rightarrow e^- + 2O_2 + 0eV$	1e-19	[15]
$O^- + CO_2 \rightarrow e^- + O + CO_2 + 0eV$	4e-18	
$O^- + CO \rightarrow e^- + O + CO + 0eV$	4e-18	
$O^- + C \rightarrow e^- + O + C + 0eV$	4e-18	
$O^- + O \rightarrow e^- + 2O + 0eV$	4e-18	
$O^- + O_2 \rightarrow e^- + O + O_2 + 0eV$	4e-18	
$O^- + O_3 \rightarrow e^- + O + O_3 + 0eV$	4e-18	
$O_3^- + CO_2 \rightarrow e^- + O_3 + CO_2 + 0eV$	2.3e-17	
$O_3^- + CO \rightarrow e^- + O_3 + CO + 0eV$	2.3e-17	

Table A.1: Continued

$O_3^- + C \rightarrow e^- + O_3 + C + 0eV$	2.3e-17	
$O_3^- + O \rightarrow e^- + O_3 + O + 0eV$	2.3e-17	
$O_3^- + O_2 \rightarrow e^- + O_3 + O_2 + 0eV$	2.3e-17	
$O_3^- + O_3 \rightarrow e^- + 2O_3 + 0eV$	2.3e-17	
<b>Ion-Ion</b>		
$O_2^- + CO_2^+ \rightarrow CO + O_2 + O + 0eV$	6e-13	[13]
$O_2^- + O^+ \rightarrow O_2 + O + 0eV$	$2.7e-13(300/T_g)^{0.5}$	[15]
$O_2^- + O_2^+ \rightarrow 2O_2 + 0eV$	$2.01e-13(300/T_g)^{0.5}$	[15]
$O_2^- + O_2^+ \rightarrow O_2 + 2O + 0eV$	4.2e-13	[15]
$O_3^- + O_2^+ \rightarrow O_3 + O_2 + 0eV$	$2e-13(300/T_g)^{0.5}$	[15]
$O_3^- + O_2^+ \rightarrow O_3 + 2O + 0eV$	$1e-13(300/T_g)^{0.5}$	[15]
$O_3^- + O^+ \rightarrow O_3 + O + 0eV$	$1e-13(300/T_g)^{0.5}$	[15]
$O^- + O^+ \rightarrow 2O + 0eV$	$4e-14(300/T_g)^{0.43}$	[15]
$O^- + O_2^+ \rightarrow O_2 + O + 0eV$	$2.6e-14(300/T_g)^{0.44}$	[15]
$O^- + O_2^+ \rightarrow 3O + 0eV$	$4.2e-13(300/T_g)^{0.44}$	[15]
<b>Ion-Neutral</b>		
$CO_2 + CO^+ \rightarrow CO_2^+ + CO + 0eV$	1e-15	[15]
$O + O_2^- \rightarrow O_2 + O^- + 0eV$	1.5e-16	[14]
$O^+ + CO_2 \rightarrow O_2^+ + CO + 0eV$	8.1e-16	[15]
$O^+ + CO_2 \rightarrow CO_2^+ + O + 0eV$	9e-17	[15]
$C^+ + CO_2 \rightarrow CO^+ + CO + 0eV$	1.1e-15	[15]
$CO^+ + CO_2 \rightarrow CO_2^+ + CO + 0eV$	1e-15	[15]
$C^+ + CO \rightarrow C + CO^+ + 0eV$	5e-19	[15]
$CO^+ + C \rightarrow CO + C^+ + 0eV$	1.1e-16	[15]

Table A.1: Continued

$O_2^+ + C \rightarrow CO^+ + O + 0eV$	5.2e-17	[15]
$O_2^+ + C \rightarrow C^+ + O_2 + 0eV$	5.2e-17	[15]
$CO_2^+ + O \rightarrow O_2^+ + CO + 0eV$	1.64e-17	[15]
$CO_2^+ + O \rightarrow O^+ + CO_2 + 0eV$	9.62e-17	[15]
$CO_2^+ + O_2 \rightarrow O_2^+ + CO_2 + 0eV$	5.3e-17	[15]
$CO^+ + O \rightarrow CO + O^+ + 0eV$	1.4e-16	[15]
$CO^+ + O_2 \rightarrow CO + O_2^+ + 0eV$	1.2e-16	[15]
$C^+ + O_2 \rightarrow CO + O^+ + 0eV$	4.54e-16	[15]
$C^+ + O_2 \rightarrow CO^+ + O + 0eV$	3.8e-16	[15]
$O^+ + O_2 \rightarrow O_2^+ + O + 0eV$	$1.9e-17(300/T_g)^{0.5}$	[15]
$O^- + O_3 \rightarrow O + O_3^- + 0eV$	5.3e-16	[15]
$O_2^- + O_3 \rightarrow O_2 + O_3^- + 0eV$	4e-16	[15]
$O^+ + O_3 \rightarrow O_2^+ + O_2 + 0eV$	1e-16	[15]
$O_3^- + O \rightarrow O_3 + O^- + 0eV$	1e-19	[15]
$O_3^- + O \rightarrow O_2^- + O_2 + 0eV$	2.5e-16	[15]
<b>Neutral-Neutral</b>		
$O + O_3 \rightarrow 2O_2 + 0eV$	$8e-18e^{-2056/T_g}$	[15]
$O_2 + C \rightarrow CO + O + 0eV$	$1.99e-16e^{-2010/T_g}$	[14]
<b>Recombination</b>		
$e^- + CO_2^+ \rightarrow CO + O + 0eV$	6.5e-13	[13]
$e^- + CO_2^+ \rightarrow C + O_2 + 0eV$	$3.94e-14T_e^{-0.4}$	
$e^- + CO^+ \rightarrow C + O + 0eV$	$3.46e-14 T_e^{-0.48}$	[14]
$e^- + C^+ \rightarrow C + 0eV$	$4.77e-18 T_e^{-0.595}$	
$e^- + O^+ \rightarrow O + 0eV$	$3.55e-18 T_e^{-0.619}$	

## BIBLIOGRAPHY

- [1] EMA®, *Ansys charge plus*, version 2024R1.
- [2] Tech. Rep., U.S. Environmental Protection Agency, "Overview of SF6 Emissions Sources and Reduction Options in Electric Power Systems." Available at <https://www.epa.gov/eps-partnership/overview-sf6-emissions-sources-and-reduction-options-electric-power-systems>. 2018. Accessed: June, 2024.
- [3] Arpa-e project: Tesla: Tough and ecological supercritical line breaker for ac, "https://arpa-e.energy.gov/technologies/projects/tesla-tough-and-ecological-supercritical-line-breaker-ac." 2022.
- [4] M. Rabie and C. Franck, "Assessment of eco-friendly gases for electrical insulation to replace the most potent industrial greenhouse gas sf6," *Environmental Science and Technology*, vol. 52, no. 2, 2017, doi:10.1021/acs.est.7b0346.
- [5] Z. Yang, S. Hosseini, T. Kiyani, S. Gnapowski, and H. Akiyama, "Post-breakdown dielectric recovery characteristics of high-pressure liquid co2 including supercritical phase," *IEEE Transactions on Dielectrics and Electrical Insulation*, vol. 21, no. 3, pp. 1089–1094, 2014, doi:10.1109/TDEI.2014.6832252.
- [6] Y. Tian, J. Wei, C. Park, Z. Wang, and L. Graber, "Modelling of electrical breakdown in supercritical co2 with molecular clusters formation," *2018 12th International Conference on the Properties and Applications of Dielectric Materials (ICPADM)*, pp. 992–995, 2018, doi:10.1109/ICPADM.2018.8401205.
- [7] L. Xingwen, T. Kari, C. Degui, S. Haitao, and X. Ensheng, "Simulation of arc motion in air switching devices taking ferromagnetic material into account," *Plasma Science and Technology*, vol. 11, no. 2, 2009, doi:10.1088/1009-0630/11/2/22.

- [8] M. Mürmann, A. Chusov, R. Fuchs, A. Nefedov, and H. Nordborg, “Modeling and simulation of the current quenching behavior of a line lightning protection device,” *Journal of Physics D: Applied Physics*, vol. 50, no. 10, 2017, doi:10.1088/1361-6463/aa560e.
- [9] A. Gleizes, I. Sakalis, M. Razafinimanana, and S. Vacquie, “Decay of wall stabilized arcs in sf6-n2 mixtures,” *Journal of Applied Physics*, vol. 61, no. 2, 1987, doi:10.1063/1.338251.
- [10] Z. F. G. Wong, N. Guo, S. M. Neall, Z. Jin, L. Graber, and J. Rauleder, “Cfd simulation and design of a new supercritical co2 circuit breaker contact and nozzle system,” in *2024 IEEE Electrical Insulation Conference (EIC)*, 2024, pp. 176–179.
- [11] V. Vahedi and M. Surendra, “A monte carlo collision model for the particle-in-cell method: Applications to argon and oxygen discharges,” *Computer Physics Communications*, vol. 87, pp. 179–198, 1994, doi:10.1016/0010-4655(94)00171-W.
- [12] E. W. Lemmon, I. H. Bell, M. L. Huber, and M. O. McLinden, *NIST Chemistry Web-Book, NIST Standard Reference Database Number 69*. National Institute of Standards and Technology, ch. Thermophysical Properties of Fluid Systems.
- [13] M. Alliat, D. Mei, and X. Tu, “Plasma activation of co2 in a dielectric barrier discharge: A chemical kinetic model from the microdischarge to the reactor scales,” *Journal of CO2 Utilization*, vol. 27, pp. 308–319, 2018.
- [14] A. Berthelot and A. Bogaerts, “Modeling of co2 plasma: Effect of uncertainties in the plasma chemistry,” *Plasma Sources Science and Technology*, vol. 26, no. 11, p. 115 002, Oct. 2017.
- [15] P. Koelman *et al.*, “A comprehensive chemical model for the splitting of co2 in non-equilibrium plasmas,” *Plasma Processes and Polymers*, vol. 14, no. 4-5, p. 1 600 155, 2017. eprint: <https://onlinelibrary.wiley.com/doi/pdf/10.1002/ppap.201600155>.

- [16] B. Gerke *et al.*, “Suppression of electrical breakdown phenomena in liquid trimethyl bismuth based ionization detectors,” *Journal of Instrumentation*, vol. 17, no. 09, P09029, Sep. 2022.
- [17] T. Yong, H. Zhong, E. Pannier, C. Laux, and M. Cappelli, “High-pressure co2 dissociation with nanosecond pulsed discharges,” *Plasma Sources Science and Technology*, vol. 32, no. 11, 2023, doi:10.1088/1361-6595/ad066e.
- [18] I. D. Boyd, “Computation of hypersonic flows using the direct simulation monte carlo method,” *Journal of Spacecraft and Rockets*, vol. 52, no. 1, pp. 38–53, 2015. eprint: <https://doi.org/10.2514/1.A32767>.
- [19] G. Sarma, “Physico–chemical modelling in hypersonic flow simulation,” *Progress in Aerospace Sciences*, vol. 36, no. 3, pp. 281–349, 2000.
- [20] T. E. Schwartzenruber and I. D. Boyd, “Progress and future prospects for particle-based simulation of hypersonic flow,” *Progress in Aerospace Sciences*, vol. 72, pp. 66–79, 2015, Celebrating 60 Years of the Air Force Office of Scientific Research (AFOSR): A Review of Hypersonic Aerothermodynamics.
- [21] E. Ching, M. Barnhardt, and M. Ihme, “Sensitivity of hypersonic dusty flows to physical modeling of the particle phase,” *Journal of Spacecraft and Rockets*, vol. 58, no. 3, pp. 653–667, 2021. eprint: <https://doi.org/10.2514/1.A34810>.
- [22] K. A. Fisco and D. R. Chapman, “Comparison Of Shock Structure Solutions Using Independent Continuum And Kinetic Theory Approaches,” in *Sensing, Discrimination, and Signal Processing and Superconducting Materials and Instrumentation*, J. A. Ionson and R. Nichols, Eds., International Society for Optics and Photonics, vol. 0879, SPIE, 1988, pp. 113–122.
- [23] L.L. Alves, ”The IST-Lisbon database on LXCat” *J. Phys. Conf. Series* 2014, 565, 1.
- [24] O. Zatsarinny and K. Bartschat 2013 *J. Phys. B: At. Mol. Opt. Phys.* 46 112001.

[25] TRINITY database, [www.lxcat.net](http://www.lxcat.net), retrieved on October 6, 2024.

[26] Hayashi database, [www.lxcat.net](http://www.lxcat.net), retrieved on October 6, 2024.